Schistosoma mansoni infection reprograms the metabolic potential of the myeloid lineage in a mouse model of metabolic syndrome

Diana Cortes-Selva[1], Lisa Gibbs[1], J. Alan Maschek [5,6], Tyler Van Ry[3,5], Bartek Rajwa[2], James E. Cox[3,5], Eyal Amiel[4], Keke C. Fairfax [1,7]

[1] Department of Pathology, Division of Microbiology and Immunology, University of Utah, Salt Lake City UT, 84112
[2] Bindley Bioscience Center, Purdue University, West Lafayette IN, 47907
[3] Department of Biochemistry, University of Utah, Salt Lake City UT, 84112
[4] Department of Biomedical and Health Sciences, University of Vermont, Burlington, VT 05405
[5]Metabolomics, Proteomics and Mass Spectrometry Cores, University of Utah, Salt Lake City, UT, 84112
[6] Department of Nutrition and Integrative Physiology and the Diabetes and Metabolism Research Center, University of Utah, Salt Lake City, UT 84112

Running title: Schistosomes reprogram myeloid metabolism

[7]Lead contact:

Keke Fairfax
Department of Pathology
Division of Microbiology and Immunology
University of Utah
JMRB 2200B
15 N Medical Drive East
Salt Lake City, UT 84112
Email: keke.fairfax@path.utah.edu
ORCID: https://orcid.org/0000-0002-8382-2960
801-581-5980 (office)

Keywords: Myeloid lineage, macrophage metabolism, *Schistosoma mansoni*, biological sex, metabolic disease

Summary

Despite evidence that helminths protect from metabolic disease, a major gap exists in understanding the underlying mechanism(s). Here we demonstrate that bone marrow derived macrophages (BMDM) from *S. mansoni* infected male ApoE$^{-/-}$ mice have dramatically increased mitochondrial respiration compared to those from uninfected mice. This change associates with increased glucose and palmitate shuttling into TCA cycle intermediates and decreased accumulation of cellular cholesterol esters. Moreover, systemic metabolic modulation by schistosomes is a function of biological sex, where infection protects ApoE$^{-/-}$ male, but not female, mice from obesity and glucose intolerance. Sex-dependence extends to myeloid cells, where reprogramming leads to opposite cholesterol phenotypes in BMDM from females and males. Finally, the metabolic reprogramming of male myeloid cells is transferrable via bone marrow transplantation to an uninfected host, indicating maintenance of reprogramming in the absence of sustained antigen exposure. This work reveals that *S. mansoni* systemic reprograming of myeloid metabolism is sex-dependent.

Introduction

Cardiovascular disease (CVD) is the leading worldwide cause of mortality (Hinton et al., 2018; Roth et al., 2017). In the United States, 65% of adults diagnosed with diabetes have elevated LDL cholesterol levels or take cholesterol lowering medications, and death rates from atherosclerotic cardiovascular disease (CVD) are ~1.7 times higher in this population as compared to non-diabetic adults (Emerging Risk Factors et al., 2010). It is well established that in the diabetic population, obesity, and dyslipidemia are risk factors underlying these increases in

mortality, while hyperglycemia is an independent risk factor (Marks and Raskin, 2000; Wong et al., 2016). Underlying conditions such as diabetes and atherosclerosis contribute to the burden of CVD in both females and males. While, the incidence of CVD is markedly higher in men than in age-matched women (Opotowsky et al., 2007; Tan et al., 2010), the risk of developing CVD while diabetic is much greater in women than men (Humphries et al., 2017; Peters et al., 2014). In non-diabetic patients, females exhibit increased insulin sensitivity in comparison to males, as well as reduced prevalence of dysglycemia and enhanced muscle glucose uptake (Cnop et al., 2003; Kim and Reaven, 2013; Moran et al., 2008; Willeit et al., 1997), suggesting sex-dependent modulations in whole body metabolism. Recent studies suggest a role of the gut microbiota in the differences between sexes in the regulation of lipid metabolism (Baars et al., 2018). Nevertheless, complete understanding of mechanistic basis behind sexual dimorphism in metabolic syndrome is still lacking.

Previous studies have uncovered an association between a history of helminth infection and reduced prevalence of metabolic disease in humans and rodents ((Doenhoff et al., 2002; Stanley et al., 2009; Wiria et al., 2015). Specifically, infection by Schistosomes reduces cholesterol and atherosclerotic plaques (Doenhoff et al., 2002; Stanley et al., 2009), this effect has been attributed, in part, to an anti-inflammatory phenotype in macrophages (Wolfs et al., 2014) and transcriptional reprogramming of phospholipid and glucose metabolism related genes in hepatic macrophages (Cortes-Selva et al., 2018). Moreover, it has been postulated that schistosomes have the potential to affect long term glucose metabolism in T cells (Chen et al., 2013). Accumulating evidence suggests that biological sex affects disease progression; yet the effect of schistosomiasis on metabolic-protection in females and males it is not well understood, as most

studies have been conducted only in males or no sex differentiation has been made during data analysis ((Sanya et al., 2019; Shen et al., 2015; Wolde et al., 2019)). To date, no report with a particular emphasis on females has been conducted.

Schistosomiasis induces Th2 polarization and alternative activation of macrophages, essential for host survival (Barron and Wynn, 2011; Fairfax et al., 2012; Herbert et al., 2004). IL-4 induced alternative activation of macrophages relies on oxidative phosphorylation (OXPHOS) and fatty acid oxidation for energy production, and is dependent on cell intrinsic lysosomal lipolysis (Huang et al., 2014; Vats et al., 2006). Macrophage metabolism follows a dysmorphic pattern, as sex-related differences affect the processes involved in cholesterol and lipid metabolism in macrophages as well as inflammatory cytokine production in adipose tissue (Griffin et al., 2016; Ng et al., 2001). Moreover, in rats, phagocytes from females had increased ROS generation than males (Rudyk et al., 2018). Such differences have often been attributed to the role of sex hormones in gene expression and immune cell function (Rubinow, 2018; Taneja, 2018; Winn et al., 2019), but a clear understanding of the effects of sex on the regulation of macrophage metabolism, as well as how sex modulates the effects of schistosomiasis in the protection from metabolic disease is lacking.

In the present study, we sought to determine the systemic effects of *S. mansoni* infection on the myeloid lineage. Surprisingly, we discovered that macrophages derived from the bone marrow of *S. mansoni* infected male mice have dramatically increased oxygen consumption and mitochondrial mass compared to those from uninfected males. This shift is accompanied by increased carbon shuttling into TCA cycle intermediates, a decrease in cholesterol esters, and

increased fatty acid oxidation. When we examined the role of biological sex in schistosome induced modulation we found that *S. mansoni* infection does not reliably protect ApoE$^{-/-}$ female mice from HFD induced weight gain or glucose intolerance. The sex-dependent effect of infection extends to the myeloid lineage, where bone marrow derived macrophages from infected females display the opposite metabolic phenotype as those from infected males, with a dramatic increase in cellular cholesterol esters. Overall, these data present the first evidence that *S. mansoni* systemically modulates the myeloid compartment in a sex-dependent manner and provide a more comprehensive understanding of how *S. mansoni* infection may confer metabolic protection at the cellular level.

Results

Macrophages derived from *S. mansoni* infected male mice have increased oxygen consumption and spare respiratory capacity

We have previously reported that schistosomiasis alters the expression of numerous genes relevant to glucose, cholesterol, and amino acid metabolism in hepatic macrophages of male mice (Cortes-Selva et al., 2018). These alterations are associated with improved insulin sensitivity and atherosclerotic score in male mice. Since it has previously been shown that during *S. mansoni* infection the majority of liver macrophages are monocyte derived, and monocyte recruitment drives both atherosclerosis (Potteaux et al., 2011; Tacke et al., 2007) and obesity induced insulin resistance (Beliard et al., 2017; Liang et al., 2007; Oh et al., 2012; Rull et al., 2010), we hypothesized that Schistosome infection may imprint the monocyte- macrophage lineage with altered metabolic propensities. To elucidate whether infection imprints

137 macrophages with an altered metabolic phenotype we infected (and mock infected controls)
138 atherogenesis-prone male ApoE$^{-/-}$mice on high-fat diet (HFD), and sacrificed them at 10-weeks
139 post-infection to harvest bone marrow cells. Macrophages were differentiated *in vitro* with M-
140 CSF in a 6-7-day culture. We performed real-time extracellular flux analysis on unstimulated
141 bone marrow derived macrophages (BMDM) from ApoE$^{-/-}$ HFD infected and uninfected
142 (control) HFD mice to quantify oxygen consumption rate (OCR) (Figure 1A). BMDM from
143 ApoE$^{-/-}$ HFD infected mice showed improved basal respiration (Figure 1B) and significantly
144 increased spare respiratory capacity ($p<0.0001$, Figure 1C). Since eukaryotic cells integrate
145 oxidative phosphorylation (OXPHOS), glycolysis and the tricarboxylic acid (TCA) cycle to
146 satisfy energy requirements, we also tested the extracellular acidification rate (ECAR), which is
147 suggested as a marker of inhibited mitochondrial respiration (Pike Winer and Wu, 2014), in
148 BMDM from infected and uninfected ApoE$^{-/-}$ HFD mice. We observed no differences in ECAR
149 in infected male mice compared to uninfected controls (Figure 1D). Cell intrinsic lysosomal
150 lipolysis has previously been shown to support macrophage spare respiratory capacity in the
151 context of macrophage alternative activation (Huang et al., 2014; Liu et al., 2017). We stained
152 for hydrophobic and neutral lipids by Oil Red O (ORO) (Mehlem et al., 2013) and observed that
153 the lipid content of BMDM from infected ApoE$^{-/-}$ males trended to reduction in comparison to
154 the control group, but was not significantly reduced (Figure 1E). To analyze BMDM
155 mitochondrial mass, which has also been linked to increased respiratory capacity (Langston et
156 al., 2017), we analyzed mitochondrial activity by Mitotracker Deep Red FM. We observed that
157 BMDM from infected mice exhibited increased MitoTracker median fluorescent intensity (MFI)
158 in comparison to the BMDM from uninfected mice (Figure 1F). Overall, these data indicate that
159 *S. mansoni* infection in males leads to increased oxygen consumption and mitochondrial

metabolism in BMDM. Mitochondrial oxidative dysfunction in macrophages has recently been linked to insulin resistance (Jung et al., 2018), so this metabolic shift could contribute to the infection-induced improvement in glucose tolerance seen in infected males .

Schistosomiasis in male ApoE$^{-/-}$ mice alters metabolic flux of glucose and the lipidomic fingerprint of macrophages

In order to understand how Schistosome infection alters the metabolic fingerprint and promotes mitochondrial metabolism in macrophages derived from ApoE$^{-/-}$ HFD male mice, we performed metabolic tracing analysis, where macrophages were differentiated in the presence of normal glucose and then switched to ^{13}C-labeled glucose for 24 hours. We observed increased shuttling of heavy labeled glucose to malate (Figure 2A), citrate (Figure 2B), itaconate (Figure 2C), and succinate Figure 2E in BMDM from infected mice in comparison to BMDM from uninfected mice. The lack of increased heavy lactate production (Figure 2D), suggests that the primary reprogramming is focused on glucose-dependent mitochondrial metabolism. Importantly, we found no upregulation of alternative activation markers (CD301, CD206, Arg1, Nos2) in unstimulated BMDM from infected mice when compared to BMDM from controls (Supplementary Figure 1). Since we have previously shown that infection alters the phospholipid and cholesterol metabolism in hepatic macrophages (Cortes-Selva et al., 2018), we performed unbiased lipidomics using liquid chromatography-mass spectrometry (LC-MS). We used a supervised model by partial least squares-discriminant analysis (PLS-DA), with two components to determine the lipidomic profile of BMDM. There was a robust separation between groups that indicates the metabolic profiles of BMDM from infected and uninfected males differ

significantly and suggests that there is a prominent alteration of metabolites induced by infection in male mice (Figure 2F). The lipid species that drive the variation observed in the PLS-DA as measured by the Variable Importance in Projection (VIP) score from uninfected males in comparison to infected males included cholesterol esters (CE) (20:1), CE (22:0), CE (24:0), CE (24:1), CE (22:4), CE (22:1), CE (18:0); diacylglycerols (DG) (16:0_16:0), DG (16:0_18:0) and triacyclglycerol (TG) (16:0_16:0_16:0) (Figure 2G,H). We then analyzed the total CE levels in macrophages from both groups of male mice and found that infection led to significantly reduced CE in male mice ($p<0.0001$, Figure 2I), further evidencing an important role of cholesterol metabolism in macrophages following helminth infection. Next, we determined the transcriptomic modifications induced by infection in unstimulated BMDM from infected and uninfected males by mRNA sequencing (mRNAseq). Significant gene expression differences were observed in BMDM from infected male mice, compared to uninfected controls. Transcripts from the two groups are depicted in Volcano plots, using false discovery rate (FDR<0.05 in red, FDR<0.01 in blue) and Log2 fold changes (cut off of .6 Log2 FC) to identify statistically significant genes (Figure 2J). Among the differentially regulated factors are Gbp6, which is related to interferon-γ signaling and innate immune function; Gm7609, a predicted pseudogene; Gbp4, a member of the GTPase family involved in protective immunity against microbial and viral pathogens; Apol9a, which is predicted to be related to lipid transport, lipoprotein metabolic processes and stimulated by interferon; Iigp1, a GTPase with roles in response to intracellular pathogens; CD300e, which belongs to families of paired activating and inhibitory receptors implicated in immune responses; and Batf2, a basic leucine zipper factor whose activation is detrimental for type-1 infectious disease. Importantly, Mgll, which encodes monoacylglycerol lipase that catalyzes the conversion of monoacylglycerides to free fatty acids and glycerol was

206 significantly increased. Mgll is required for lipolysis and improved glucose homeostasis in mice
207 on HFD (Berdan et al., 2016; Douglass et al., 2015), an infection driven increase was validated
208 by RT-qPCR (Figure 2L). In addition, Slc1a3, which encodes for the glutamate aspartate
209 transporter 1 that is localized in the inner mitochondria membrane as part of the malate-aspartate
210 shuttle and is relevant for amino acid homeostasis in adipocytes, was significantly altered in our
211 model, and was further validated by RT-qPCR (Figure 2M). Interestingly, the pathways
212 significantly altered (Figure 2K) during infection included hematopoietic cell lineage ($p=5.779$
213 $x10^{-8}$), asthma ($p=3.169\ x10^{-5}$), and cytokine-cytokine receptor interactions, graft-versus host
214 disease, type 1 diabetes and allograft regression ($p=0.0000894$). Together, these data identify key
215 factors in immune and metabolic responses as well as novel factors with unknown functions that
216 are regulated by exposure to *S. mansoni* infection.
217
218 **_S. mansoni_ infection protects male mice, but not female mice, from obesity and glucose**
219 **intolerance independently of systemic alternative macrophage activation**
220
221 Sex is a key contributor to the phenotype of cardiovascular and metabolic features in mammals
222 (Chella Krishnan et al., 2018), so we assessed the sex dependent impact of *S. mansoni* infection
223 on obesity and glucose intolerance. For this, we fed male and female $ApoE^{-/-}$ HFD for 10-days
224 before infection. We infected and mock infected mice (controls) as described in the methods.
225 Ten weeks post infection we analyzed body weight and glucose tolerance (via an IP glucose
226 tolerance test) and found that infection is significantly beneficial for male, but not female mice,
227 as only males are protected from HFD-induced weight gain and glucose intolerance (Figure 3A,
228 3B). We also analyzed serum triglyceride (TG) and diglyceride (DG) levels using untargeted

lipidomics and found that relative abundance of both TG and DG were decreased in infected males as compared to uninfected males, while TGs were increased by infection in females and DGs were unchanged (Figure 3C). These data indicate that *S. mansoni* infection induces a sex-dependent modulation of metabolic disease parameters. We then wondered if this infection-mediated effect in males only was correlated with differences in systemic alternative activation of hepatic macrophages in females. Flow cytometry analysis showed that alternative activation markers (CD206, CD301, Arg1) were highly expressed in macrophages from male and female mice following infection, but not in naïve mice (Figure 3D), suggesting that *S. mansoni* induced alternative activation irrespective of sex. Previous studies characterizing the dynamics of alternatively activated macrophages during schistosome infection have found that these macrophages primarily arise from $Ly6C^{high}$ monocytes (Girgis et al., 2014; Nascimento et al., 2014). Naïve male and female $ApoE^{-/-}$ mice on HFD had equivalent frequencies of $Ly6c^{high}$ monocytes circulating in peripheral blood. At 10-weeks post infection we found an increased percentage of both $Ly6C^{int}$ and $Ly6C^{high}$ cells (Figure 3E) in both male and female mice compared to the mock infected controls, with the frequency of $Ly6C^{high}$ cells in females 1.74 times that of males, suggesting either increased monopoiesis in females, or increased tissue recruitment in males . Since we had found increased mitochondrial MFI in BMDM from infected male mice, we asked whether circulating blood monocytes are similarly modulated. We observed an infection induced increase in Mitotracker fluorescent intensity in monocytes from male $ApoE^{-/-}$ mice on HFD, but not from females (Figure 3F). These data suggest that there is sex-specific increased mitochondrial activity following infection in the monocyte cell population. We then wondered if these effects in the differentiated monocytes are the result of long-lasting changes in the myeloid lineage after helminth infection. For this, we analyzed the main lineages of

hematopoietic progenitors that produce myeloid cells: granulocyte-monocyte progenitors (GMP), monocyte-DC progenitors (MDP) and the common myeloid progenitor (CMP) in female and male ApoE$^{-/-}$ mice. CMP were defined as Lin^{-}CD127^{-}c-Kit^{+}Sca-1^{-}CD34^{+}FcRII/III$^{lo/-}$(Paul et al., 2016), GMP were defined as Lin^{-}IL-7R^{-}Sca-1^{-}c-kit^{+}CD34^{+}FcR II/III^{+}, and MDP were defined as defined as Lin^{-} c-Kit^{+} Sca-1^{-} CD34^{+} FcγR^{lo} CD115^{hi} cells. Overall bone marrow cellularity was not affected by Schistosome infection (Figure 3G), however, the numbers of CMP and GMP in infected male mice were significantly reduced compared to uninfected controls, while GMP and CMP were not reduced in females (Figure 3 H-J). The numbers and percentages of MDP remained unchanged in infected females and males compared to uninfected controls (Figure 3K, 3L). These data suggest that *S. mansoni* infection modulates both metabolic disease and the myeloid lineage in a sex-specific manner that is independent from the induction of systemic alternative activation.

S. mansoni-increases fatty acid oxidation in male but not female ApoE$^{-/-}$ mice on HFD

In order to determine whether infection-induced pathologic differences in males and females were accompanied by sex-specific differential macrophage metabolic regulation, we cultured bone marrow cells from 10-week infected or uninfected control male and female mice for 7 days to generate BMDM. OCR was measured in real time in basal conditions and following the addition of mitochondrial inhibitors in unstimulated BMDM from both infected and uninfected male and female ApoE$^{-/-}$ animals. Similar to as seen in Figure 1A, BMDM from infected males exhibited increased basal OCR and spare respiratory capacity compared to uninfected male controls (Figure 4A, 4B, 4C). However, basal OCR and spare respiratory capacity of BMDM

from infected females remained unaltered in comparison to BMDM from uninfected females (Figure 4A, 4B, 4C). Moreover, side by side OCR analysis in females and males with palmitate as a substrate (glucose limiting conditions) showed that BMDM from infected male, but not from infected females had an increased ability to oxidize exogenous palmitate (Figure 4D). In addition, BMDM from infected males but not females had significantly increased palmitate basal OCR and palmitate spare respiratory capacity, suggesting exogenous free fatty usage as a carbon source for OXPHOS (Figure 4E, 4F). Similar to the male only data, we observed no differences in macrophage lipid content in either group, suggesting that global lipolysis may not underlie OCR and spare respiratory capacity in our model (Figure 4G). Additionally, analysis of mitochondrial mass in females and males showed that similar to blood monocytes, BMDM from infected male mice, but not females have a significantly higher Mitotracker MFI. These data suggest that *S. mansoni* infection improved mitochondrial biogenesis in males, but not females. Again, suggesting differential regulation of macrophage metabolism based on biological sex. This regulation may account in part for the differences in the role of infection in modulating obesity and insulin sensitivity.

S. mansoni infection differentially alters the cellular lipid profile in female and male mice

To understand the sex specific modulations induced by schistosomiasis in macrophage lipid metabolism, we isolated cellular lipids from unstimulated BMDM and performed unbiased lipidomics in male and female derived-cells. PLS-DA showed that *S. mansoni* infection led to a sex-specific lipid profile (Figure 5A). Further, analysis of total CE (identified as a VIP species in males in Figure 2) showed that infection led to decreased levels of CE in cells derived from

298 infected male mice. In contrast, infection led to significantly increased total CE in BMDM
299 derived from infected female mice (Figure 5B). Similar to males, infection in females induces a
300 unique lipid signature (Figure 5C), with two species of plasmanyl-PE, three species of
301 plasmanyl-PC, BMP and CE as the main drivers of the altered lipid profile in females during
302 infection (Figure 5D). Since we observed BMP's as a VIP compound driven by *S. mansoni*
303 infection in females, but not males, we went back and performed targeted lipidomics to quantify
304 BMPs at the class level. Indeed, total BMPs were significantly increased by infection in BMDM
305 from females but not males (Figure 5E). Our Seahorse data indicates that *S. mansoni* infection
306 induced differential oxidation of exogenous palmitate in BMDM derived from males and
307 females. In order to understand the metabolic flux of exogenous palmitate, we performed
308 metabolic tracing analysis of palmitate, where macrophages were differentiated in the presence
309 of normal glucose and then switched to C^{13}-labeled palmitate for 24 hours. Similar to what we
310 documented with glucose, we observed increased shuttling of heavy labeled palmitate into
311 succinate, malate, and fumarate in BMDM derived from infected males, with decreased shuttling
312 into myristate (a marker of fatty acid elongation). BMDM derived from infected females
313 displayed the opposite phenotype, with decreased shuttling of heavy labeled palmitate into
314 succinate, malate, and fumarate, and increased shuttling into myristate compared to BMDM from
315 uninfected controls. These data suggest that BMDM derived from infected male $ApoE^{-/-}$ mice
316 have increased basal utilization of exogenous palmitate for beta-oxidation, while the female data
317 suggests increased lipid synthesis, strengthening the data obtained from our palmitate
318 extracellular flux analysis.
319 To further understand the role of biological sex in the *S. mansoni* induced reprograming of the
320 BMDM lipidome, we isolated cellular lipids from male and female BMDM either unstimulated

(media), or following LPS stimulation, and then performed untargeted lipidomics as described in Figure 5. We analyzed the lipidomic data with machine learning using a two-step selection process (see Methods). This approach identified ~20 features (lipid compounds) contributing to an elastic net regression model that can predict the infection status of samples-originating animals (Zou, 2005). These informative features are listed in descending order of importance (Supplemental Figure 2A). Interestingly, some key features (for instance, the top scoring one) are not represented as significant in the univariate tests (univariate adjusted p values, Supplemental Figure 2B). However, these features are important contributors to the multivariate machine learning model. This is not unexpected – some features that would be considered uninformative individually may be very useful in improving predictions if combined with other features. When we examine these features individually, we can see a differential response to infection for males and females (for instance, PG 18:1_18:2, a glycerophospholipid) represented in Supplemental Figure 2C). Seven of the 20 molecular features identified by machine learning are BMP (Bis(monoacylglycerol)phosphate) species, which have been implicated in glycosphingolipid degradation and cholesterol transport (Anheuser et al., 2019; Luquain-Costaz et al., 2013). These data further support the hypothesis that *S. mansoni* infection differentially modulates the metabolism of myeloid cells from male and female animals, and that this modulation revolves around decreased cholesterol storage and fatty acid synthesis in males and increased cholesterol storage and fatty acid synthesis in females. Cholesterol and lipid metabolism has previously been associated with inflammatory myeloid effector function (Carroll et al., 2018; Funk et al., 1993; Oiknine and Aviram, 1992), so we quantified the acute inflammatory effectors nitrite and iNOS, along with pro-inflammatory cytokines/chemokines IL-12p70, CXCL1, and IL-6 (chemokines/cytokines with known pathogenic roles in obesity, insulin resistance and

344 atherosclerosis) following stimulation with LPS. *S. mansoni* infection increases LPS induced
345 nitrite and iNOS production in BMDM from male, but not female ApoE$^{-/-}$ mice on HFD (Figure
346 5 J,K). Conversely, BMDM from infected males have decreased production of IL-2p70, CXCL1,
347 and IL-6 (Figure 5 L-N) following LPS stimulation as compared to BMDM from uninfected
348 controls. LPS induced IL-12p70, CXCL1, and IL-6 production by female BMDM is unaffected
349 by infection status. Increased production of the effector molecules nitrite and iNOS combined
350 with decreased production of pro-inflammatory mediators associated with chronic inflammation
351 supports the idea that *S. mansoni* infection promotes a hybrid macrophage state in males.
352
353 **_S. mansoni_ infection modulates the myeloid transcriptome in a sex-specific manner**
354 Since we documented significant sex dependent shifts in functional metabolism in BMDM from
355 male and female *S. mansoni* infected mice, we sought to determine if differential transcriptional
356 modulation underlies these shifts. In order to investigate the genes and respective pathways that
357 were associated with specific conditions and the ones that were differentially regulated by sex we
358 performed mRNAseq on unstimulated BMDM derived from male and female ApoE$^{-/-}$ mice at 10-
359 weeks post *S. mansoni* or mock infection. We identified different subsets of genes that were
360 preferentially upregulated in males ($p<0.05$, Figure 6A). Among 1448 genes upregulated in
361 males regardless of infection status with a p value <0.05, the majority of these (238 genes) were
362 associated to metabolic functions by pathway analysis. Of these 238 genes involved in
363 metabolism we identified hexokinase 1 (hk1), citrate synthase (cs), apolipoprotein A2 (apoa2),
364 aldehyde dehydrogenase 3 family member A2 (aldh3a2), lipoyltransferase (lipt1), solute carrier
365 family 19 member 1 (slc19a1), LDL receptor related protein 1 (lrp1), many of these are involved
366 in lipoprotein and cholesterol metabolism. These data suggest that myeloid metabolism is

differentially regulated by sex, at least in the context of HFD. In addition, we found 216 genes involved in immunity. Among these genes with immune function we identified interleukin 10 (il-10), Toll like receptor 5 (tlr5), NLR family pyrin domain containing 3 (nlrp3), inducible T cell costimulatory (icos), which have diverse pro and anti-inflammatory function in the immune system. Next, we surveyed the genes that are differentially regulated in males and females following *S. mansoni* infection. We found 66 genes involved in metabolism, hemostasis, the adaptive immune system, collagen degradation and not annotated to specific pathways. Following the genes with known function, the majority (10) of differentially regulated genes have documented roles in metabolism. Among these, we identified type II iodothyronine deiodinase (dio2), which has been implicated in the regulation of diet induced obesity (Kurylowicz et al., 2015; Vernia et al., 2013). Moreover, we found that hexokinase 3 (hk3), fatty acid binding protein 4 (fabp4), sphingomyelin synthase 2 (sgms2), solute carrier family 6 member 8 (slc6a8) were all upregulated in male and downregulated in female BMDM following *S. mansoni* infection (Figure 6B). In addition, we performed gene ontology analysis from the 66 genes that were differentially regulated in females and males. The most significant pathways were response to glucocorticoids, glycoprotein metabolism, and fatty acid metabolism, again suggesting that there is a sex-specific metabolic response to *S. mansoni* infection in myeloid cells. These pathways may help explain the differential metabolic modulation induced by schistosomiasis in males and females (Figure 6C).

S. mansoni induced modulation of male macrophage metabolism is long-lived in the absence of antigen

Our metabolic and transcriptomic data from BMDM differentiated *in vitro* from male *S. mansoni* infected mice suggested that metabolic modulation may be long-lived in the absence of ongoing antigen exposure. In order to determine durable nature of modulation we transferred bone marrow from either 10-week *S. mansoni* infected male ApoE$^{-/-}$ mice on HFD, or uninfected male controls into busulfan treated recipient ApoE$^{-/-}$ mice on HFD. At 10 weeks post-bone marrow transfer we assayed glucose tolerance via an i.p. GTT. Mice that received bone marrow from infected males have a significantly lower glucose area under the curve (AUC) than those that received control bone marrow. We harvested bone marrow from all recipients and differentiated BMDM in M-CSF for 6 days and then performed real-time extracellular flux analysis. BMDM from recipients of bone marrow from *S. mansoni* infected mice had significantly higher basal oxygen consumption and a trend towards increased spare respiratory capacity as compared to BMDM generated from recipients of uninfected control bone marrow. Additionally, BMDM from recipients of bone marrow from *S. mansoni* infected mice had a significantly higher Mitotracker MFI than BMDM from recipients of control bone marrow. These data suggest that *S. mansoni* induced metabolic modulation of the myeloid lineage in males is long-lived even in the absence of ongoing exposure to egg antigens, and that hematopoietic cells are at least partially responsible for the regulation of whole-body glucose metabolism in the HFD ApoE$^{-/-}$ model.

Discussion

Helminth infections in general, and schistosomiasis in specific, have been known to be inversely correlated with obesity and glucose intolerance for over a decade, a phenomenon thought to be associated with Type 2 polarization of macrophages and T cells. In the current study we report that *S. mansoni* infection induces dramatic metabolic alterations in BMDM from male ApoE$^{-/-}$ mice on HFD. Our results indicate that macrophages derived from the bone marrow

412 of infected male mice have increased basal oxygen consumption and spare respiratory capacity
413 compared to those derived from uninfected males. In T cells, an increase in spare respiratory
414 capacity has been linked to mitochondrial biogenesis, and controls the transition to a long-lived
415 memory phenotype (van der Windt et al., 2012). In macrophages, M2 (alternative) activation has
416 previously been shown to lead to increased spare respiratory capacity, a process that also
417 involves mitochondrial biogenesis (Kannan et al., 2016), while TLR recognition of bacteria has
418 been shown to increase mitochondrial respiration via modulation of complex I and II (Garaude et
419 al., 2016) . In both cell types, the increased mitochondrial respiration underlies the longevity of
420 the cells. In our model we have not found most of the traditional markers used to define M2
421 alternative activation by flow cytometry at steady state (Supplemental Figure 1). Arg1 is the only
422 canonical M2 transcript that is modulated in the BMDM from infected male mice at steady state,
423 and that fold increase is relatively low (.894 log FC, adjusted *p*-value =.035). Arg1 drives the
424 production of polyamines, which in turn are able to modulate mitochondrial OxPHOS (Galvan-
425 Pena and O'Neill, 2014; Puleston et al., 2019). In the currently accepted paradigm of M2
426 polarization stat6 phosphorylation upregulates PGC1-β and PPARγ, leading to mitochondrial
427 biogenesis and increased beta-oxidation in addition to Arg1transcription. Here we present a
428 model where neither PGC1-β or PPARγ are modulated, but Arg1 transcription is increased with
429 a concomitant dramatic increase in mitochondrial respiration, suggesting that there may be
430 alternative ways to modulate mitochondrial metabolism.

431 Alternative activation has previously been shown to be dependent on cell intrinsic
432 lysosomal lipolysis and lal, with the defining feature being reductions in lipid droplets (Huang et
433 al., 2014). In our model using unstimulated BMDM from *S. mansoni* infected mice there is no
434 gross difference in lipid droplets, nor an increase in lal transcripts. Instead, we found a

435 significant shift in the lipidome of BMDM from infected male mice that centered on a reduction
436 in cholesterol esters. Previously published work in IL-4 induced M2 macrophages has found that
437 lipolysis centered on TGs as a fatty acid source. While we did find reductions in two species of
438 DGs and one species of monoacylglycerol (MG), there were no significant alterations to TAGs
439 in the BMDM generated from infected males. Flux analysis with heavy carbon labeled glucose
440 and palmitate suggest that BMDM from male infected mice have increased shuttling of both
441 glucose and palmitate into TCA cycle intermediates, suggesting that these cells have increased
442 mitochondrial beta oxidation. In addition to the unique lipidomic modulations, we found that the
443 dramatic increase in both basal oxygen consumption and spare respiratory capacity we observed
444 in BMDM from male infected mice was significantly palmitate dependent. This observation
445 further supports the idea that *in vivo* exposure of myeloid precursors to helminth antigens
446 induces unique metabolic modulations that focus on cholesterol and lipid metabolism as a source
447 for palmitate for beta oxidation. These data suggest that hybrid metabolic states in the absence of
448 M1 or M2 polarization occur in macrophages in the context of chronic disease, and present a
449 challenge to the dichotomy of M1 versus M2 activation being driven by immunometabolism.
450 Future studies exploring the immunometabolism of bone marrow derived and tissue resident
451 macrophages and dendritic cells from other chronic infections and inflammatory diseases are
452 needed in order to obtain a true picture of the correlation between metabolism and myeloid
453 polarization.

454 There are significant clinical differences in both the etiology and pathology of diabetes
455 and cardiovascular disease between males and females, but sex differences in immunological
456 activation or modulation by *S. mansoni* infection have not previously been studied in humans or
457 animal models. Surprisingly, we found that the unique metabolic modulations induced by *S.*

458 *mansoni* infection in BMDM from male mice do not occur in females, and infected females are
459 not reliably protected from high-fat diet induced obesity or glucose intolerance. Interestingly,
460 hepatic macrophage alternative activation in response to infection is equivalent between males
461 and females, but infection increases blood monocyte frequency in females to a much greater
462 extent than in males, suggesting sex specific modulation of either monopoiesis or monocyte
463 recruitment into tissues. Blood monocytes from infected males phenocopy the increase in
464 Mitotracker MFI that we have found in BMDM generated from infected males, indicating that
465 our BMDM model is likely an accurate representation of the *in vivo* potential of the myeloid
466 compartment. Interestingly, we found that infection significantly reduced the total number of
467 CMP and GMP in male, but not female bone marrow, again pointing to a sex-specific
468 modulation of the myeloid lineage at the precursor level. The reduction of CMP and GMP in
469 infected males suggests either an increase in the rate of differentiation into
470 monocytes/granulocytes, or decreased homeostatic proliferation. Since males have fewer blood
471 monocytes than female, we favor the later possibility. These possibilities and the relationship
472 between reductions in numbers of CMP and GMP in males, and the functional metabolic
473 differences in BMDM will be explored in future work.
474
475 Analysis of the BMDM transcriptomes from males and females revealed that over a
476 thousand genes are up regulated in male versus female BMDM regardless of *S. mansoni*
477 infection state. At the same time, over five dozen are differentially regulated by infection.
478 Focusing on the genes that are up-regulated in BMDM from infected males and down-regulated
479 in females, we found more than ten genes with known functions in cellular metabolism. Some of
480 these genes, like PFKFB3, have known regulatory elements for progesterone and estrogen (Shi et

al., 2017), but some of them, like fabp4, have no published mechanism of sex hormone regulation. Glycolysis and cholesterol metabolism have previously been shown to directly affect the inflammatory potential of myeloid cells. Our data indicate that *S. mansoni* infection induces a hybrid inflammatory state in male but not female BMDM, where the LPS induced production of nitrite and iNOS is enhanced, while the production of the key chronic pro-inflammatory mediators IL-12p70, CXCL1, and IL-6 are reduced. This inflammatory profile is distinct from what has previously been published with IL-4 induced M2 macrophages, where the production of iNOS and nitrite are reduced following TLR stimulation (Lam et al., 2016). CXCL1 and IL-6 have previously been linked to increased monocyte recruitment and disease progression in both atherosclerosis and obesity-induced diabetes (Boisvert et al., 2006; Hartman and Frishman, 2014; Nunemaker et al., 2014; Qu et al., 2014; Zhou et al., 2011), so these data support the possibility of infection driven modulation of macrophage function supporting the decreased pathology seen in infected males. We have demonstrated that the modulation of macrophage oxygen consumption is transferrable to an uninfected recipient, and can last for at least ten weeks, suggesting that in males, *S. mansoni* infection induces long-lived metabolic modulation of the myeloid lineage that survives in the absence of ongoing antigenic exposure. Trained innate immunity has previously been documented to be induced by BCG immunization (Kaufmann et al., 2018), and has recently been suggested to be the mechanism underlying the association between previous bacterial and fungal infections and the development of atherosclerosis (Hoogeveen et al., 2018; Leentjens et al., 2018). In these models, trained immunity and epigenetic reprogramming is driven in part from a switch from oxidative phosphorylation to increased aerobic glycolysis (Cheng et al., 2014; Stienstra et al., 2017). In the case of BCG, trained circulating monocytes can be found months after immunization, which strongly suggests

reprogramming of bone marrow progenitors (Ifrim et al., 2014). Recent reports indicate that western high-fat diet itself also induces innate training of bone marrow progenitors in both the $Ldr^{-/-}$ model of atherosclerosis (Christ et al., 2018) and in obesity related steatohepatitis (Krenkel et al., 2020). Our data suggests that *S. mansoni* infection in males trains the myeloid lineage in the opposite fashion; modulating the metabolic transcriptome of the myeloid lineage such that oxidative phosphorylation and mitochondrial activity is increased, while the chronic inflammatory potential is decreased. Alterations to the numbers and frequency of myeloid progenitors and the transferability of our phenotype via bone marrow suggests that progenitors are indeed modulated in our model, the relative role of epigenetic modulation versus microRNA regulation in dictating the *S. mansoni* induced myeloid transcriptome will be the subject of future studies.

There are significant differences in both the susceptibility and disease presentation between males and females for both diabetes and cardiovascular disease, but few studies have focused on the role of immunometabolism in this dichotomy. Our data suggests apparent biological sex-dependent differences in both the ability of schistosomes to protect from the development of HFD induced metabolic disease parameters, and the ability to modulate macrophage glucose and lipid metabolism. The current epidemiological data strongly indicates an inverse correlation between helminth infections and metabolic diseases such as diabetes and cardiovascular disease, but these studies were not designed to identify sex-specific correlations. Few animal studies have focused on the role of myeloid cells in driving sex-specific metabolic differences. Our current data indicate a clear need for further studies in both humans and animal models to specifically probe the relationship between biological sex and myeloid metabolism, and how chronic helminth infections modulate this.

Conflict of Interest

The authors declare no competing interests.

Acknowledgements

The work was supported by The University of Utah, a Scientist Development Grant from the American Heart Association to KCF (14SDG18230012), an American Heart Association Pre-doctoral Award (18PRE34030086) to DCS, and 1R21AI135385-01A1 to EA. *B. glabrata* snails provided by the NIAID Schistosomiasis Resource Center of the Biomedical Research Institute (Rockville, MD) through NIH-NIAID Contract HHSN272201700014I for distribution through BEI Resources. JEC is supported through U54 DK110858-01, mass spectrometry equipment employed was provided by 1S10OD016232-01, 1S10OD018210-01A1 and 1S10OD021505-01 to JEC.

STAR Methods

KEY RESOURCES TABLE

REAGENT or RESOURCE	SOURCE	IDENTIFIER
Antibodies		
Anti-mouse F4/80 (Clone: BM8)	Biolegend	Cat no. 123114
Anti-mouse CD64 a and b Alloantigens (Clone: X54-5/7.1.1)	BD Biosciences	Cat no. 558455
Biotinylated Goat Anti-m-Mer	R&D Systems	Cat no. BAF591
Anti-mouse CD11c (Clone: N418)	BioLegend	Cat no. 117306
Rat Anti-mouse I-A/I-E (Clone: M5/114.15.2)	BD Biosciences	Cat no. 562366
Anti-mouse Ly6A/E (Sca-1) (Clone: D7)	eBiosciences	Cat no.17-5981-82
Rat anti-mouse CD117/c-kit	R&D Systems	Cat no. FAB1356
Anti-mouse CD115 (Clone: AFS98)	eBiosciences	Cat no. 25-1152-82
Anti-mouse CD16/32 (Clone: 93)	Invitrogen	Cat no.25-0161-82
Anti-mouse CD4 (Clone: GK1.5)	BioLegend	Cat no.100406
Anti-mouse CD206 (Clone:C06C2)	BioLegend	Cat no. 141721
Rat Anti-mouse CD301	BioRad	Cat no. MCA2392A488
Anti-mouse Nos2 (Clone: CXNFT)	Invitrogen	Cat no. 46-5920-80

Anti Hu/Mo Arg1 (Clone: A1exF5)	Invitrogen	Cat no.48-3697-80
Anti-mouse CD19 (Clone: MB19-1)	Invitrogen	Cat no.11-0191-85
Anti-mouse Ter119 (Clone: Ter-119)	Invitrogen	Cat no. 11-5921082
Rat Anti-mouse Ly6G and Ly6C (Clone: RB6-8C5)	BD Biosciences	Cat no. 553127
Anti-mouse CD3 (Clone: 17A2)	BioLegend	Cat no. 100204
Anti-mouse Ly6C (Clone: HK1.4)	Invitrogen	Cat no. 45-5932-82
Anti-mouse CD45 (Clone 30-F11)	Biolegend	Cat no.103154
Anti-mouse CD11b (Clone: M1/70)	eBiosciences	Cat no. 56-0112-82
MitoTracker™ Deep Red FM	Invitrogen	Cat no. M22426
Anti-mouse CD34 (Clone: SA376A4)	BioLegend	Cat no.152203
TrueStain fcX (anti-mouse CD16/32) (Clone: 93)	BioLegend	Cat no.101320
Anti-mouse CD127 (Clone: A7R34)	BioLegend	Cat no. 135043
Biological Samples		
Fetal Bovine Serum	ThermoFisher	Cat no. 10091148
Chemicals, Peptides, and Recombinant Proteins		
Endotoxin free LPS (Escherichia coli Serotype O)	InvivoGen	Cat no. tlrl-eblps
D-Glucose-^{13}C6	Sigma Aldrich	Cat no. 389374
Recombinant murine M-CSF	Peprotech	Cat no. 315-03
BD Pharm Lyse Lysing Buffer	BD Biosciences	Cat no. 555899
Taqman Gene Expression Master Mix	Applied Biosystems	Cat no.4369016
Trypan Blue solution	Sigma	T81154-100ML
Streptavidin APC	BD Biosciences	Cat no. 554067
Streptavidin APC/Fire 750	Biolegend	Cat no.405250
Streptavidin PE	BD Biosciences	Cat no. 554061
Streptavidin PB	Invitrogen	Cat no. S11222
Streptavidin PE-Cy5	BD Biosciences	Cat no. 554062
(Ethylenedinitrilo)tetraacetic acid (EDTA)	Thermo Fisher Scientific	Cat no. AM9260G
Fixation/Permeabilization		
Collagenase	Sigma Aldrich	Cat no. 5138
Trizol LS Reagent	Ambion	Cat no. 10296028
Chloroform	Alfa Aesar	Cat no. 32614
Glucose	Sigma Aldrich	Cat no. G7528
2-Propanol	Fisher Chemical	Cat no. A416
Critical Commercial Assays		
Seahorse Bioassay	Agilent Technologies	Cat no.102416
SuperScript IV-VILO Master Mix	Thermo Fisher	Cat no.11766050
RNA Clean and Concentrator Kit	Zymo Research	Cat no. 11-353
Zombie Red Fixable Viability Kit	BioLegend	Cat no.423109
^{13}C Glucose	Santa Cruz Biotech	Cat no. 106032-62-6
^{13}C Palmitate	Sigma-Aldrich	Cat no. 605573
Cellstripper cell dissociation reagent	Corning	Cat no. 25-056-CI

Western High-fat diet	Envigo	TD 88137
Deposited Data		
GEO	https://www.ncbi.nlm.nih.gov/geo/	GSE144447
Experimental Models: Organisms/Strains		
B6.129P2-Apoetm1Unc/J	The Jackson Laboratory	Stock No: 002052
Parasite: *Schistosoma mansoni*	Biomedical Research Institute	https://www.afbr-bri.org/schistosomiasis/ordering/
Software and Algorithms		
FlowJo Software X 10.0.7r2	BD Biosciences	https://www.flowjo.com/solutions/flowjo/downloads/previous-versions
GraphPad Prism 8.2.0	GraphPad	https://www.graphpad.com/support/faq/prism-820-release-notes/
Attune NxT Accoustic Focusing Cytometer	Invitrogen	https://www.thermofisher.com/us/en/home/life-science/cell-analysis/flow-cytometry/flow-cytometers/attune-acoustic-focusing-flow-cytometer.html
iPathways Guide	Advaita	https://advaitabio.com/ipathwayguide/
MH Qual	Agilent Technologies, Inc	https://www.agilent.com/en/products/software-informatics/masshunter-suite/masshunter/masshunter-software
MassHunter Quantitative Analysis B.07.00	Agilent Technologies, Inc	https://www.agilent.com/en/products/software-informatics/masshunter-suite/masshunter/masshunter-software
LipidMatch	University of Florida	http://secim.ufl.edu/secim-tools/lipidmatch/
MetaboAnalyst 3.0	Xia et al., 2015	http://www.metaboanalyst.ca
Other		

Mgll Taqman Gene Expression Assay	ThermoFisher	Assay ID: Mm00449274_m1
Slc1a3 Taqman Gene Expression Assay	ThermoFisher	Assay ID: Mm00600697_m1.
Beta actin Taqman Gene Expression Assay	ThermoFisher	Assay ID: Mm00607939_s1

LEAD CONTACT AND MATERIALS AVAILABILITY

Further information requests should be directed to and will be fulfilled by the Lead Contact, Keke Fairfax (keke.fairfax@path.utah.edu). These studies generated no new reagents.

EXPERIMENTAL MODEL AND SUBJECT DETAILS

Parasite and Mouse Models

This study was carried out in accordance with the recommendations in the Guide for the Care and Use of Laboratory Animals of the National Institutes of Health. The protocols were approved by the Institutional Animal Care and Use Committees of the University of Utah and Purdue University. Snails infected with *S. mansoni* (strain NMRI, NR-21962) were provided by the Schistosome Research Reagent Resource Center for distribution by BEI Resources, NIAID NIH. Male and female ApoE$^{-/-}$ (B6.129P2-Apoetm1Unc/J) were purchased from the Jackson Laboratories and bred at the University of Utah. Mice were housed in pathogen-free conditions and were fed standard rodent chow (2019 rodent chow, Harlan Teklad) until 10-14 days before infection when they were transitioned to a high-fat diet (HFD: 21% milk fat, 0.15% cholesterol: TD 88137 Envigo). Bone marrow chimeras were generated by treating ApoE$^{-/-}$ mice that had been on high- fat diet for 4 weeks with 20mg/kg of pharmaceutical grade busulfan for 5 days (total dose of 100mg/kg). On day 6 mice were i.v. injected with 2.5-3 x 10^6 bone marrow cells from either 10-week *S. mansoni* infected or control uninfected ApoE$^{-/-}$ mice on high-fat diet.

562 Reconstitution was validated via flow-cytometry at 3-weeks post-transfer and recipient mice
563 were maintained on high-fat diet for 10-weeks post-reconstitution.

564 **METHOD DETAILS**

565 ***S. mansoni* infection and glucose tolerance test**

566 ApoE$^{-/-}$ female and male mice of 6 weeks of age were exposed percutaneously to 75-90 cercariae
567 of *S. mansoni* or were mocked infected (as controls). At five- and ten-weeks post-infection mice
568 were fasted for 5 hours and baseline blood glucose levels were obtained via lateral tail vein nick.
569 Mice were then administered a single intraperitoneal injection of glucose (2mg/g of body weight,
570 ultrapure glucose, Sigma G7528). Blood glucose levels were obtained at 20, 60, and 90 min post
571 injection. Individual data points obtained were analyzed by Area Under Curve (AUC).

572

573 **Mouse macrophage culture**

574 Mouse bone marrow-derived macrophages (BMDM) were generated as follows: bone marrow
575 cells were isolated by centrifugation of bones at >10,000 x g in a microcentrifuge tube for 15
576 seconds as previously described (Amend et al., 2016). Cells were differentiated in M-CSF
577 (20ng/mL, Peprotech, Rocky Hill, NJ) in complete macrophage medium (CMM: RPMI1640,
578 10% FCS, 2mM L-glutamine and 1 IU/mL Pen-Strep for 6 or 7 days. On the last day, cells
579 were harvested in Cellstripper cell dissociation reagent (Corning) were washed with CMM) and
580 prepared for downstream assays.

581

582 **Glycolytic and phospho-oxidative metabolism measurement (seahorse assay)**

583 BMDM from different conditions (uninfected controls or *S. mansoni* infected) were resuspended
584 at the same concentration in XF assay media supplemented with 5% FCS and 5mM glucose. The

day before the assay, the probe plate was calibrated and incubated at 37 C in a non-CO2 incubator. Resuspended cells were seeded at a concentration of $1.5x10^5$ cells per well and incubated for 20-60 minutes in the Prep Station incubator (37 C non-CO2 incubator). Following initial incubation, XF Running Media (XF assay media with 5% FCS and 10mM Glucose) were dispensed into each well. OCR and ECAR were measured by an XF96 Seahorse Extracellular Flux Analyzer following the manufacturer's instructions. For the seahorse assay, cells were treated with oligomycin (1uM), FCCP (1.5uM), rotenone (100nM) and antimycin A (1uM). Each condition was performed in 2-3 technical replicates. For determination of palmitate dependent respiration, BSA-conjugated palmitate (BSA: palmitate = 1:6, molar ratio) was prepared according to the Seahorse protocol (Seahorse Bioscience). Briefly, 1 mM sodium palmitate (Sigma Aldrich) was conjugated with 0.17 mM fatty acid free-BSA (Sigma Aldrich) in 150 mM NaCl solution at 37°C for 1h. Palmitate-BSA was stored in glass vials at -20°C until use. Cells were incubated as above in glucose limited XF media per manufacturer instructions.

Flow Cytometry

Livers from uninfected and infected mice were perfused with 1X PBS, mashed and digested in DMEM 0.5% Collagenase (Sigma) at 37°C for 15 min. Then, livers were mashed and filtered through a 100 μm metal strainer and digested an additional 15 min. Following second digestion, the liver contents were strained, washed with DMEM and spun down 1500 rpm for 5 min. The pellet was lysed with 1X lysis buffer (BD PharmLyse), quenched with 1% FBS DMEM, and washed to be used in flow cytometry. Surface staining was performed using the following mAb against mouse antigens: CD45 (30-F11, eBioscience), CD301(BioRad), CD206 (C068C2, Biolegend), F4/80 (BM8, Biolegend), mouse Mer biotinylated (R&D), CD64(X54-5/7.1, BD).

Intracellular antigen staining such as Nos2 (CXNFT, Invitrogen, and C-11, Santa Cruz) and Arg1 (Invitrogen, A1exF5)) was performed using the Intracellular Fixation and Permeabilization Buffer set (Thermo Fisher Scientific cat. no. 88-8824) per manufacturer's instruction. Further, bone marrow cells were obtained by centrifugation of bones into tubes at >10000 rpm for 15 s. Surface staining for bone marrow precursors was performed using the following antibodies: Ter119, CD19, CD4, CD3, Gr-1, CD11b, Sca-1, CD115, Ly6C, c-Kit, flt3, CD127 and CD16/32. PBMC from whole blood were obtained following red blood cell lysis and used for flow cytometry analysis. Surface staining of PBMC was performed using Ter119, CD64, CD11b, CD115, Ly6C and MitoTracker Red.

Samples were acquired using Attune NxT Focusing Flow Cytometer (Thermo Fisher Scientific) and analyzed using Flowjo X 10.0.7r2 (FlowJo LLC, Inc.).

RNA Isolation and q-RT-PCR

BMDM were stored in Trizol, and RNA isolation was performed as described in the Immunological Genome Project Total RNA isolation protocol. Next, cDNA was synthesized from RNA using Superscript IV VILO (ThermoFisher Scientific) for reverse transcription. qPCR was performed using TaqMan Gene expression assays (Mgll, Slc1a3, beta actin, ThermoFisher) on an Applied Biosystems Stepone Plus Real-Time PCR System. Beta-Actin assay number Mm00607939_s1, mgll assay Mm00449274_m1, slc1a3 assay Mm00600697_m1. Relative expression was calculated using the 2-ΔΔCt method.

Measurement of Cytokines and Inflammatory mediators

For cytokine levels of BMDCs, supernatants were collected at 24 hours post stimulation and measured with Mouse Cytokine and Chemokine ProcartaPlex 26plex panel (Life Technologies) per manufacture instructions using a Luminex Magpix system. Nitrite levels in cell culture media were determined using a Griess reagent kit for nitrite determination (Invitrogen) according the manufacturer's instructions.

Untargeted lipidomics

Sample extraction from serum or cell pellets

Lipids were extracted from serum (50µL) or cell pellets in a combined solution as described in (Matyash et al., 2008). In detail, samples were combined in solution with 225 µL MeOH containing internal standards (IS; Avanti splash Lipidomix (Lot#12), 10µL each sample) and 750 µL methyl tert-butyl ether (MTBE). The samples were sonicated for 1 min, rested on ice for 1 hour, briefly vortexed every 15 min then an addition of 200µL dd-H2O was made to induce phase separation. All solutions were pre-chilled on ice. The sample were then vortexed for 20 s, rested at room temperature for 10 min, and centrifuged at 14,000 g for 10 min at 4 C. The upper organic phase was collected and evaporated to dryness under vacuum. Lipid samples were reconstituted in 200µL IPA and transferred to an LC-MS vial with insert for analysis. Concurrently, a process blank sample was brought forward as well as quality control sample was prepared by taking equal volumes (10µL per sample) from each sample after final resuspension.

LC-MS Methods

Lipid extracts were separated on a Waters Acquity UPLC CSH C18 1.7 um 2.1 x 100 mm column maintained at 65 °C connected to an Agilent HiP 1290 Sampler, Agilent 1290 Infinity

pump, equipped with an Agilent 1290 Flex Cube and Agilent 6530 Accurate Mass Q-TOF dual ESI mass spectrometer. For positive mode, the source gas temperature was set to 225 °C, with a gas flow of 11 L/min and a nebulizer pressure of 50 psig. VCap voltage was set at 3500 V, fragmentor at 110 V, skimmer at 85 V and Octopole RF peak at 750 V. For negative mode, the source gas temperature was set at 325 °C, with a drying gas flow of 12 L/min and a nebulizer pressure of 30 psig. VCap voltage is set 3000 V, fragmentor at125 V, skimmer at 75 V and Octopole RF peak at 750 V. Reference masses in positive mode (*m/z* 121.0509 and 922.0098) were infused with nebulizer pressure at 2 psig, in negative mode reference masses (*m/z* 1033.988, 966.0007, 112.9856 and 68.9958) were infused with a nebulizer pressure at 5psig. Samples were analyzed in a randomized order in both positive and negative ionization modes in separate experiments acquiring with the scan range m/z 100-1700. Mobile phase A consisted of ACN:H_2O (60:40 *v/v*) in 10 mM ammonium formate and 0.1% formic acid, and mobile phase B consisted of IPA:ACN:H_20 (90:9:1 *v/v*) in 10 mM ammonium formate and 0.1% formic acid. The chromatography gradient for both positive and negative modes started at 15% mobile phase B then increased to 30% B over 2.4 min, then increased to 48% from 2.4-3.0 min, followed by an increase to 82% B from 3-13.2 min, and then to 99% from 13.2-13.8 min where it was held until 15.4 min and then returned to the initial conditioned and equilibrated for 4 min. Flow was 0.5 mL/min throughout, injection volume was 5µL for positive and 7 µL negative mode. Tandem mass spectrometry is conducted using the same LC gradient at collision energies of 20 V and 40 V.

Targeted lipidomics

Sample Preparation

Lipids were extracted from cell pellets (500,000 cells) as described in detail above (Matyash et al., 2008). For targeted lipidomics, lipid extracts were separated on a Waters BEH HILIC column 1.7 µm, 100 mm × 3 mm column maintained at 60 °C connected to an Agilent HiP 1290 Sampler, Agilent 1290 Infinity pump, and equipped with an Agilent 6490 triple quadrupole (QqQ) mass spectrometer. Lipids were detected using dynamic multiple reaction monitoring (dMRM) in negative ion mode. Source gas temperature is set to 225 °C, with a gas flow of 13 L/min and a nebulizer pressure of 30 psi. Sheath gas temperature was 350 °C, sheath gas flow was 11 L/min, capillary voltage of 4000 V, nozzle voltage was 500 V, high pressure RF was 190 V and low-pressure RF was 120 V. Injection volume was 2 µL and the samples were injected in a randomized order. Mobile phase A consisted of H_2O, mobile phase B consisted of ACN:H_2O (96:4 *v/v*) and both contain 7 mM ammonium acetate. The chromatography gradient started at 100% mobile phase B and decreased to 84% B over 10 min. Post-time was 9 min and the flow rate was 0.4 mL/min throughout. Collision energies (25 V) and cell accelerator voltages (3 V) were optimized using lipid standards with dMRM quantifier transitions as $[M-H]^- \rightarrow [T2\_RCOO]^-$ and qualifier transitions of $[M-H]^- \rightarrow [T1\_RCOO]^-$ and $[M-H]^- \rightarrow [NL\_T2Ketene]^-$.

Lipid data analysis

The pooled QC samples and process blank samples were injected throughout the sample queue to ensure the reliability of acquired LC-MS data. Results from LC-MS experiments were collected using Agilent MassHunter (MH) Workstation and analyzed using the software packages MH Qual, MH Quant (Agilent Technologies, Inc) and LipidMatch to prepare the data set.

The data table exported from MHQuant was evaluated using Excel where initial lipid targets were parsed based on the following criteria. Only lipids with relative standard deviation (RSD)

699 less than 30% in QC samples were used for data analysis. Additionally, targets identified in
700 blanks or double blanks at significant amounts (area under the curve (AUC) target blank/AUC
701 target QC >30%) were removed from analysis. Lipids were quantitated based on peak area ratios
702 to the spiked IS of the same or nearest class.
703
704 **RNA Sequencing**
705 Library Preparation and sequencing
706 The concentration and quality of total RNA samples was first assessed using Agilent 2100
707 Bioanalyzer. A RIN (RNA Integrity Number) of five or higher was required to pass the quality
708 control. Then 200 nanograms of RNA per sample were used to prepared dual-indexed strand-
709 specific cDNA library using KAPA mRNA Hyperprep Kit (Roche). The resulting libraries were
710 assessed for its quantity and size distribution using Qubit and Agilent 2100 Bioanalyzer. Two
711 hundred pico molar pooled libraries were utilized per flowcell for clustering amplification on
712 cBot using HiSeq 3000/4000 PE Cluster Kit and sequenced with 2.75bp paired-end configuration
713 on HiSeq4000 (Illumina) using HiSeq 3000/4000 PE SBS Kit. A Phred quality score (Q score)
714 was used to measure the quality of sequencing. More than 90% of the sequencing reads reached
715 Q30 (99.9% base call accuracy).
716
717 Sequence alignment and gene counts
718 The sequencing data were first assessed using FastQC (Babraham Bioinformatics, Cambridge,
719 UK) for quality control. Then all sequenced libraries were mapped to the mouse genome (UCSC
720 mm10) using STAR RNA-seq aligner (Dobin et al., 2013) with the following parameter: "--
721 outSAMmapqUnique 60". The reads distribution across the genome was assessed using bamutils

(from ngsutils) (Breese and Liu, 2013). Uniquely mapped sequencing reads were assigned to mm10 refGene genes using featureCounts (from subread) (Liao et al., 2014) with the following parameters: "-s 2 –p –Q 10". Quality control of sequencing and mapping results was summarized using MultiQC (Ewels et al., 2016). Genes with read count per million (CPM) > 0.5 in more than 2 of the samples were kept. The data was normalized using TMM (trimmed mean of M values) method. Differential expression analysis was performed using edgeR (McCarthy et al., 2012; Robinson et al., 2010). False discovery rate (FDR) was computed from p-values using the Benjamini-Hochberg procedure.

Pathway analysis

The Data (significantly impacted pathways, biological processes, molecular interactions.) were analyzed using Advaita Bio's iPathwayGuide (http://www.advaitabio.com/ipathwayguide). Pathway analysis was performed on $\log_2$-transformed data using Bonferroni-corrected *p*-values. The data discussed in this publication have been deposited in NCBI's Gene Expression Omnibus (Edgar *et al*., 2002) and are accessible through GEO Series accession number GSE 144447(https://www.ncbi.nlm.nih.gov/geo/query/acc.cgi?acc=GSE144447)

Heavy glucose and heavy palmitate labeling

For metabolomics tracing in Figure 2 BMDM were differentiated in CMM containing normal glucose. At Day 6 of culture cells were switched to CMM containing $^{13}C_6$-glucose (Santa Cruz Biotech) for 24 hours. Cells were harvested and processed as described below. For metabolomics tracing in figure 5 BMDM were differentiated in CMM containing normal glucose and serum. At Day 6 of culture cells were switched to CMM containing dialyzed serum and 1 mM ^{13}C palmitate (sigma Aldrich) for 36 hours. Cells were harvested and processed as described below.

745
746

747 **Metabolomics**

748 *Extraction*

749 Cold 90% methanol (MeOH) solution was added to each sample to give a final concentration of
750 80% MeOH to each cell pellet. Samples were incubated at -20 °C for 1 hr. After incubation, the
751 samples were centrifuged at 20,000 x g for 10 minutes at 4 °C. The supernatant was transferred
752 from each sample tube into a labeled, fresh micro centrifuge tube. The samples were dried *en*
753 *vacuo*.

754

755 *Mass Spectrometry Analysis of Samples*

756 All GC-MS analysis was performed with an Agilent 7200 GC-QTOF and an Agilent 7693A
757 automatic liquid sampler. Dried samples were suspended in 40 µL of a 40 mg/mL O-
758 methoxylamine hydrochloride (MOX) (MP Bio #155405) in dry pyridine (EMD Millipore
759 #PX2012-7) and incubated for one hour at 37 °C in a sand bath. 25 µL of this solution was
760 added to auto sampler vials followed by the automatic addition of 60 µL of N-methyl-N-
761 trimethylsilyltrifluoracetamide (MSTFA with 1%TMCS, Thermo #TS48913) and incubated for
762 30 minutes at 37 °C. Following incubation, each sample were vortexed and 1 µL of the prepared
763 sample was injected into the gas chromatograph inlet in the split mode with the inlet temperature
764 held at 250 °C. A 10:1 split ratio was used for analysis for the majority of metabolites. Any
765 metabolites that saturated the instrument at the 10:1 split was analyzed at a 50:1 split ratio. The
766 gas chromatograph had an initial temperature of 60 °C for one minute followed by a 10°C/min
767 ramp to 325 °C and a hold time of 10 minutes. A 30-meter Agilent Zorbax DB-5MS with 10 m

768 Duraguard capillary column was employed for chromatographic separation. Helium was used as
769 the carrier gas at a rate of 1 mL/min.
770
771 *Data Analysis*
772 The area under the curve for each isotope was extracted using MHQuant software (Agilent). This
773 data was exported as a .csv file and isotopically corrected using an in house modified version of
774 DeuteRater (Naylor et al., 2017)
775
776 **Machine Learning**
777 The selection of the most informative or important features (i.e., the features contributing to the
778 prediction) was performed using a machine-learning approach involving an elastic-net regressor,
779 which followed a round of traditional univariate filtering. The process included two steps:

780 1. Creating a series of ANOVA models (one for each of the lipid-based features), and pre-
781 selecting features based on η^2 to limit the complexity of the downstream elastic net
782 model. The uninformative features were rejected and not used in the second step.
783 2. Establishing an elastic net regression model via cross-validation and grid-search of the
784 parameters. The zero coefficients of the model were removed. The top 20 non-zero
785 coefficients provided ranking for the features in terms of their importance.

786 The elastic net regression attempts to minimize the following functional:

787 $$\hat{\beta} = \underset{\beta}{\operatorname{argmin}}\left(\left|\left| y - X\beta \right|\right|^2 + \lambda\left((1-\alpha)\left|\left|\beta\right|\right|^2 / 2 + \alpha\left|\left|\beta\right|\right|_1 \right) \right)$$

788 over a grid of α and λ values (Zou, 2005). The elastic-net approach linearly combines the L_1 and
789 L_2 penalties used in LASSO (Tibshirani, 1996) and ridge-regression methods (Hoerl, 1970),

790 respectively. Therefore, the elastic net penalty would become LASSO penalty for $\alpha = 1$ and ridge
791 penalty for $\alpha = 0$. The parameter λ controls the overall strength of the combined penalty term.
792 The input X in the model consists of all the molecular features identified, and y is probability of
793 observing a particular animal.
794
795 **Statistical Analysis**
796 Statistical analyses of data were performed using one-way ANOVA, a non-parametric Mann-
797 Whitney test, or unpaired Student's t-test depending on the data distribution. $P \leq 0.05$ were
798 considered statistically significant. Analyses and graphing were performed using Prism
799 (GraphPad v8.0) and R-language for statistical computing.
800
801
802 **References**
803
804 Amend, S.R., Valkenburg, K.C., and Pienta, K.J. (2016). Murine Hind Limb Long Bone Dissection
805 and Bone Marrow Isolation. J Vis Exp.
806 Anheuser, S., Breiden, B., and Sandhoff, K. (2019). Membrane lipids and their degradation
807 compounds control GM2 catabolism at intralysosomal luminal vesicles. J Lipid Res *60*, 1099-
808 1111.
809 Baars, A., Oosting, A., Lohuis, M., Koehorst, M., El Aidy, S., Hugenholtz, F., Smidt, H., Mischke,
810 M., Boekschoten, M.V., Verkade, H.J., et al. (2018). Sex differences in lipid metabolism are
811 affected by presence of the gut microbiota. Sci Rep *8*, 13426.
812 Barron, L., and Wynn, T.A. (2011). Macrophage activation governs schistosomiasis-induced
813 inflammation and fibrosis. European journal of immunology *41*, 2509-2514.
814 Beliard, S., Le Goff, W., Saint-Charles, F., Poupel, L., Deswaerte, V., Bouchareychas, L., Huby, T.,
815 and Lesnik, P. (2017). Modulation of Gr1(low) monocyte subset impacts insulin sensitivity and
816 weight gain upon high-fat diet in female mice. Int J Obes (Lond) *41*, 1805-1814.
817 Berdan, C.A., Erion, K.A., Burritt, N.E., Corkey, B.E., and Deeney, J.T. (2016). Inhibition of
818 Monoacylglycerol Lipase Activity Decreases Glucose-Stimulated Insulin Secretion in INS-1
819 (832/13) Cells and Rat Islets. PloS one *11*, e0149008.
820 Boisvert, W.A., Rose, D.M., Johnson, K.A., Fuentes, M.E., Lira, S.A., Curtiss, L.K., and Terkeltaub,
821 R.A. (2006). Up-regulated expression of the CXCR2 ligand KC/GRO-alpha in atherosclerotic

822 lesions plays a central role in macrophage accumulation and lesion progression. The American
823 journal of pathology *168*, 1385-1395.
824 Breese, M.R., and Liu, Y. (2013). NGSUtils: a software suite for analyzing and manipulating next-
825 generation sequencing datasets. Bioinformatics *29*, 494-496.
826 Carroll, R.G., Zaslona, Z., Galvan-Pena, S., Koppe, E.L., Sevin, D.C., Angiari, S., Triantafilou, M.,
827 Triantafilou, K., Modis, L.K., and O'Neill, L.A. (2018). An unexpected link between fatty acid
828 synthase and cholesterol synthesis in proinflammatory macrophage activation. The Journal of
829 biological chemistry *293*, 5509-5521.
830 Chella Krishnan, K., Mehrabian, M., and Lusis, A.J. (2018). Sex differences in metabolism and
831 cardiometabolic disorders. Curr Opin Lipidol *29*, 404-410.
832 Chen, Y., Lu, J., Huang, Y., Wang, T., Xu, Y., Xu, M., Li, M., Wang, W., Li, D., Bi, Y., et al. (2013).
833 Association of previous schistosome infection with diabetes and metabolic syndrome: a cross-
834 sectional study in rural China. The Journal of clinical endocrinology and metabolism *98*, E283-
835 287.
836 Cheng, S.C., Quintin, J., Cramer, R.A., Shepardson, K.M., Saeed, S., Kumar, V., Giamarellos-
837 Bourboulis, E.J., Martens, J.H., Rao, N.A., Aghajanirefah, A., et al. (2014). mTOR- and HIF-1alpha-
838 mediated aerobic glycolysis as metabolic basis for trained immunity. Science *345*, 1250684.
839 Christ, A., Gunther, P., Lauterbach, M.A.R., Duewell, P., Biswas, D., Pelka, K., Scholz, C.J.,
840 Oosting, M., Haendler, K., Bassler, K., et al. (2018). Western Diet Triggers NLRP3-Dependent
841 Innate Immune Reprogramming. Cell *172*, 162-175 e114.
842 Cnop, M., Havel, P.J., Utzschneider, K.M., Carr, D.B., Sinha, M.K., Boyko, E.J., Retzlaff, B.M.,
843 Knopp, R.H., Brunzell, J.D., and Kahn, S.E. (2003). Relationship of adiponectin to body fat
844 distribution, insulin sensitivity and plasma lipoproteins: evidence for independent roles of age
845 and sex. Diabetologia *46*, 459-469.
846 Cortes-Selva, D., Elvington, A.F., Ready, A., Rajwa, B., Pearce, E.J., Randolph, G.J., and Fairfax,
847 K.C. (2018). Schistosoma mansoni Infection-Induced Transcriptional Changes in Hepatic
848 Macrophage Metabolism Correlate With an Athero-Protective Phenotype. Front Immunol *9*,
849 2580.
850 Dobin, A., Davis, C.A., Schlesinger, F., Drenkow, J., Zaleski, C., Jha, S., Batut, P., Chaisson, M.,
851 and Gingeras, T.R. (2013). STAR: ultrafast universal RNA-seq aligner. Bioinformatics *29*, 15-21.
852 Doenhoff, M.J., Stanley, R.G., Griffiths, K., and Jackson, C.L. (2002). An anti-atherogenic effect of
853 Schistosoma mansoni infections in mice associated with a parasite-induced lowering of blood
854 total cholesterol. Parasitology *125*, 415-421.
855 Douglass, J.D., Zhou, Y.X., Wu, A., Zadroga, J.A., Gajda, A.M., Lackey, A.I., Lang, W., Chevalier,
856 K.M., Sutton, S.W., Zhang, S.P., et al. (2015). Global deletion of MGL in mice delays lipid
857 absorption and alters energy homeostasis and diet-induced obesity. J Lipid Res *56*, 1153-1171.
858 Emerging Risk Factors, C., Sarwar, N., Gao, P., Seshasai, S.R., Gobin, R., Kaptoge, S., Di
859 Angelantonio, E., Ingelsson, E., Lawlor, D.A., Selvin, E., et al. (2010). Diabetes mellitus, fasting
860 blood glucose concentration, and risk of vascular disease: a collaborative meta-analysis of 102
861 prospective studies. Lancet *375*, 2215-2222.
862 Ewels, P., Magnusson, M., Lundin, S., and Kaller, M. (2016). MultiQC: summarize analysis results
863 for multiple tools and samples in a single report. Bioinformatics *32*, 3047-3048.

Fairfax, K.C., Amiel, E., King, I.L., Freitas, T.C., Mohrs, M., and Pearce, E.J. (2012). IL-10R blockade during chronic schistosomiasis mansoni results in the loss of B cells from the liver and the development of severe pulmonary disease. PLoS pathogens *8*, e1002490.

Funk, J.L., Feingold, K.R., Moser, A.H., and Grunfeld, C. (1993). Lipopolysaccharide stimulation of RAW 264.7 macrophages induces lipid accumulation and foam cell formation. Atherosclerosis *98*, 67-82.

Galvan-Pena, S., and O'Neill, L.A. (2014). Metabolic reprograming in macrophage polarization. Front Immunol *5*, 420.

Garaude, J., Acin-Perez, R., Martinez-Cano, S., Enamorado, M., Ugolini, M., Nistal-Villan, E., Hervas-Stubbs, S., Pelegrin, P., Sander, L.E., Enriquez, J.A., et al. (2016). Mitochondrial respiratory-chain adaptations in macrophages contribute to antibacterial host defense. Nature immunology *17*, 1037-1045.

Girgis, N.M., Gundra, U.M., Ward, L.N., Cabrera, M., Frevert, U., and Loke, P. (2014). Ly6C(high) monocytes become alternatively activated macrophages in schistosome granulomas with help from CD4+ cells. PLoS pathogens *10*, e1004080.

Griffin, C., Lanzetta, N., Eter, L., and Singer, K. (2016). Sexually dimorphic myeloid inflammatory and metabolic responses to diet-induced obesity. American journal of physiology. Regulatory, integrative and comparative physiology *311*, R211-216.

Hartman, J., and Frishman, W.H. (2014). Inflammation and atherosclerosis: a review of the role of interleukin-6 in the development of atherosclerosis and the potential for targeted drug therapy. Cardiol Rev *22*, 147-151.

Herbert, D.R., Holscher, C., Mohrs, M., Arendse, B., Schwegmann, A., Radwanska, M., Leeto, M., Kirsch, R., Hall, P., Mossmann, H., et al. (2004). Alternative macrophage activation is essential for survival during schistosomiasis and downmodulates T helper 1 responses and immunopathology. Immunity *20*, 623-635.

Hinton, W., McGovern, A., Coyle, R., Han, T.S., Sharma, P., Correa, A., Ferreira, F., and de Lusignan, S. (2018). Incidence and prevalence of cardiovascular disease in English primary care: a cross-sectional and follow-up study of the Royal College of General Practitioners (RCGP) Research and Surveillance Centre (RSC). BMJ Open *8*, e020282.

Hoerl, A.a.K., RW (1970). Ridge Regression: Biased Estimation for Nonorthogonal Problems. Technometrics *12*, 55-67.

Hoogeveen, R.M., Nahrendorf, M., Riksen, N.P., Netea, M.G., de Winther, M.P.J., Lutgens, E., Nordestgaard, B.G., Neidhart, M., Stroes, E.S.G., Catapano, A.L., et al. (2018). Monocyte and haematopoietic progenitor reprogramming as common mechanism underlying chronic inflammatory and cardiovascular diseases. Eur Heart J *39*, 3521-3527.

Huang, S.C., Everts, B., Ivanova, Y., O'Sullivan, D., Nascimento, M., Smith, A.M., Beatty, W., Love-Gregory, L., Lam, W.Y., O'Neill, C.M., et al. (2014). Cell-intrinsic lysosomal lipolysis is essential for alternative activation of macrophages. Nature immunology *15*, 846-855.

Humphries, K.H., Izadnegahdar, M., Sedlak, T., Saw, J., Johnston, N., Schenck-Gustafsson, K., Shah, R.U., Regitz-Zagrosek, V., Grewal, J., Vaccarino, V., et al. (2017). Sex differences in cardiovascular disease - Impact on care and outcomes. Front Neuroendocrinol *46*, 46-70.

Ifrim, D.C., Quintin, J., Joosten, L.A., Jacobs, C., Jansen, T., Jacobs, L., Gow, N.A., Williams, D.L., van der Meer, J.W., and Netea, M.G. (2014). Trained immunity or tolerance: opposing

functional programs induced in human monocytes after engagement of various pattern recognition receptors. Clin Vaccine Immunol *21*, 534-545.

Jung, S.B., Choi, M.J., Ryu, D., Yi, H.S., Lee, S.E., Chang, J.Y., Chung, H.K., Kim, Y.K., Kang, S.G., Lee, J.H., et al. (2018). Reduced oxidative capacity in macrophages results in systemic insulin resistance. Nat Commun *9*, 1551.

Kannan, Y., Perez-Lloret, J., Li, Y., Entwistle, L.J., Khoury, H., Papoutsopoulou, S., Mahmood, R., Mansour, N.R., Ching-Cheng Huang, S., Pearce, E.J., et al. (2016). TPL-2 Regulates Macrophage Lipid Metabolism and M2 Differentiation to Control TH2-Mediated Immunopathology. PLoS pathogens *12*, e1005783.

Kaufmann, E., Sanz, J., Dunn, J.L., Khan, N., Mendonca, L.E., Pacis, A., Tzelepis, F., Pernet, E., Dumaine, A., Grenier, J.C., et al. (2018). BCG Educates Hematopoietic Stem Cells to Generate Protective Innate Immunity against Tuberculosis. Cell *172*, 176-190 e119.

Kim, S.H., and Reaven, G. (2013). Sex differences in insulin resistance and cardiovascular disease risk. J Clin Endocrinol Metab *98*, E1716-1721.

Krenkel, O., Hundertmark, J., Abdallah, A.T., Kohlhepp, M., Puengel, T., Roth, T., Branco, D.P.P., Mossanen, J.C., Luedde, T., Trautwein, C., et al. (2020). Myeloid cells in liver and bone marrow acquire a functionally distinct inflammatory phenotype during obesity-related steatohepatitis. Gut *69*, 551-563.

Kurylowicz, A., Jonas, M., Lisik, W., Jonas, M., Wicik, Z.A., Wierzbicki, Z., Chmura, A., and Puzianowska-Kuznicka, M. (2015). Obesity is associated with a decrease in expression but not with the hypermethylation of thermogenesis-related genes in adipose tissues. J Transl Med *13*, 31.

Lam, R.S., O'Brien-Simpson, N.M., Holden, J.A., Lenzo, J.C., Fong, S.B., and Reynolds, E.C. (2016). Unprimed, M1 and M2 Macrophages Differentially Interact with Porphyromonas gingivalis. PloS one *11*, e0158629.

Langston, P.K., Shibata, M., and Horng, T. (2017). Metabolism Supports Macrophage Activation. Front Immunol *8*, 61.

Leentjens, J., Bekkering, S., Joosten, L.A.B., Netea, M.G., Burgner, D.P., and Riksen, N.P. (2018). Trained Innate Immunity as a Novel Mechanism Linking Infection and the Development of Atherosclerosis. Circ Res *122*, 664-669.

Liang, C.P., Han, S., Senokuchi, T., and Tall, A.R. (2007). The macrophage at the crossroads of insulin resistance and atherosclerosis. Circ Res *100*, 1546-1555.

Liao, Y., Smyth, G.K., and Shi, W. (2014). featureCounts: an efficient general purpose program for assigning sequence reads to genomic features. Bioinformatics *30*, 923-930.

Liu, P.S., Wang, H., Li, X., Chao, T., Teav, T., Christen, S., Di Conza, G., Cheng, W.C., Chou, C.H., Vavakova, M., et al. (2017). alpha-ketoglutarate orchestrates macrophage activation through metabolic and epigenetic reprogramming. Nat Immunol *18*, 985-994.

Luquain-Costaz, C., Lefai, E., Arnal-Levron, M., Markina, D., Sakai, S., Euthine, V., Makino, A., Guichardant, M., Yamashita, S., Kobayashi, T., et al. (2013). Bis(monoacylglycero)phosphate accumulation in macrophages induces intracellular cholesterol redistribution, attenuates liver-X receptor/ATP-Binding cassette transporter A1/ATP-binding cassette transporter G1 pathway, and impairs cholesterol efflux. Arterioscler Thromb Vasc Biol *33*, 1803-1811.

Marks, J.B., and Raskin, P. (2000). Cardiovascular risk in diabetes: a brief review. J Diabetes Complications *14*, 108-115.

Matyash, V., Liebisch, G., Kurzchalia, T.V., Shevchenko, A., and Schwudke, D. (2008). Lipid extraction by methyl-tert-butyl ether for high-throughput lipidomics. J Lipid Res *49*, 1137-1146.

McCarthy, D.J., Chen, Y., and Smyth, G.K. (2012). Differential expression analysis of multifactor RNA-Seq experiments with respect to biological variation. Nucleic Acids Res *40*, 4288-4297.

Mehlem, A., Hagberg, C.E., Muhl, L., Eriksson, U., and Falkevall, A. (2013). Imaging of neutral lipids by oil red O for analyzing the metabolic status in health and disease. Nat Protoc *8*, 1149-1154.

Moran, A., Jacobs, D.R., Jr., Steinberger, J., Steffen, L.M., Pankow, J.S., Hong, C.P., and Sinaiko, A.R. (2008). Changes in insulin resistance and cardiovascular risk during adolescence: establishment of differential risk in males and females. Circulation *117*, 2361-2368.

Nascimento, M., Huang, S.C., Smith, A., Everts, B., Lam, W., Bassity, E., Gautier, E.L., Randolph, G.J., and Pearce, E.J. (2014). Ly6Chi monocyte recruitment is responsible for Th2 associated host-protective macrophage accumulation in liver inflammation due to schistosomiasis. PLoS pathogens *10*, e1004282.

Naylor, B.C., Porter, M.T., Wilson, E., Herring, A., Lofthouse, S., Hannemann, A., Piccolo, S.R., Rockwood, A.L., and Price, J.C. (2017). DeuteRater: a tool for quantifying peptide isotope precision and kinetic proteomics. Bioinformatics *33*, 1514-1520.

Ng, M.K., Jessup, W., and Celermajer, D.S. (2001). Sex-related differences in the regulation of macrophage cholesterol metabolism. Curr Opin Lipidol *12*, 505-510.

Nunemaker, C.S., Chung, H.G., Verrilli, G.M., Corbin, K.L., Upadhye, A., and Sharma, P.R. (2014). Increased serum CXCL1 and CXCL5 are linked to obesity, hyperglycemia, and impaired islet function. J Endocrinol *222*, 267-276.

Oh, D.Y., Morinaga, H., Talukdar, S., Bae, E.J., and Olefsky, J.M. (2012). Increased macrophage migration into adipose tissue in obese mice. Diabetes *61*, 346-354.

Oiknine, J., and Aviram, M. (1992). Increased susceptibility to activation and increased uptake of low density lipoprotein by cholesterol-loaded macrophages. Arterioscler Thromb *12*, 745-753.

Opotowsky, A.R., McWilliams, J.M., and Cannon, C.P. (2007). Gender differences in aspirin use among adults with coronary heart disease in the United States. J Gen Intern Med *22*, 55-61.

Paul, F., Arkin, Y., Giladi, A., Jaitin, D.A., Kenigsberg, E., Keren-Shaul, H., Winter, D., Lara-Astiaso, D., Gury, M., Weiner, A., et al. (2016). Transcriptional Heterogeneity and Lineage Commitment in Myeloid Progenitors. Cell *164*, 325.

Peters, S.A., Huxley, R.R., and Woodward, M. (2014). Diabetes as risk factor for incident coronary heart disease in women compared with men: a systematic review and meta-analysis of 64 cohorts including 858,507 individuals and 28,203 coronary events. Diabetologia *57*, 1542-1551.

Pike Winer, L.S., and Wu, M. (2014). Rapid analysis of glycolytic and oxidative substrate flux of cancer cells in a microplate. PLoS One *9*, e109916.

Potteaux, S., Gautier, E.L., Hutchison, S.B., van Rooijen, N., Rader, D.J., Thomas, M.J., Sorci-Thomas, M.G., and Randolph, G.J. (2011). Suppressed monocyte recruitment drives macrophage removal from atherosclerotic plaques of Apoe-/- mice during disease regression. The Journal of clinical investigation *121*, 2025-2036.

Puleston, D.J., Buck, M.D., Klein Geltink, R.I., Kyle, R.L., Caputa, G., O'Sullivan, D., Cameron, A.M., Castoldi, A., Musa, Y., Kabat, A.M., et al. (2019). Polyamines and eIF5A Hypusination Modulate Mitochondrial Respiration and Macrophage Activation. Cell Metab *30*, 352-363 e358.

Qu, D., Liu, J., Lau, C.W., and Huang, Y. (2014). IL-6 in diabetes and cardiovascular complications. British journal of pharmacology *171*, 3595-3603.

Robinson, M.D., McCarthy, D.J., and Smyth, G.K. (2010). edgeR: a Bioconductor package for differential expression analysis of digital gene expression data. Bioinformatics *26*, 139-140.

Roth, G.A., Johnson, C., Abajobir, A., Abd-Allah, F., Abera, S.F., Abyu, G., Ahmed, M., Aksut, B., Alam, T., Alam, K., et al. (2017). Global, Regional, and National Burden of Cardiovascular Diseases for 10 Causes, 1990 to 2015. J Am Coll Cardiol *70*, 1-25.

Rubinow, K.B. (2018). An intracrine view of sex steroids, immunity, and metabolic regulation. Mol Metab *15*, 92-103.

Rudyk, M.P., Pozur, V.V., Voieikova, D.O., Hurmach, Y.V., Khranovska, N.M., Skachkova, O.V., Svyatetska, V.M., Fedorchuk, O.G., Skivka, L.M., Berehova, T.V., et al. (2018). Sex-based differences in phagocyte metabolic profile in rats with monosodium glutamate-induced obesity. Sci Rep *8*, 5419.

Rull, A., Camps, J., Alonso-Villaverde, C., and Joven, J. (2010). Insulin resistance, inflammation, and obesity: role of monocyte chemoattractant protein-1 (or CCL2) in the regulation of metabolism. Mediators Inflamm *2010*.

Sanya, R.E., Webb, E.L., Zziwa, C., Kizindo, R., Sewankambo, M., Tumusiime, J., Nakazibwe, E., Oduru, G., Niwagaba, E., Kabuubi Nakawungu, P., et al. (2019). The effect of helminth infections and their treatment on metabolic outcomes: results of a cluster-randomised trial. Clinical infectious diseases : an official publication of the Infectious Diseases Society of America.

Shen, S.W., Lu, Y., Li, F., Shen, Z.H., Xu, M., Yao, W.F., Feng, Y.B., Yun, J.T., Wang, Y.P., Ling, W., et al. (2015). The potential long-term effect of previous schistosome infection reduces the risk of metabolic syndrome among Chinese men. Parasite immunology *37*, 333-339.

Shi, L., Pan, H., Liu, Z., Xie, J., and Han, W. (2017). Roles of PFKFB3 in cancer. Signal Transduct Target Ther *2*, 17044.

Stanley, R.G., Jackson, C.L., Griffiths, K., and Doenhoff, M.J. (2009). Effects of Schistosoma mansoni worms and eggs on circulating cholesterol and liver lipids in mice. Atherosclerosis *207*, 131-138.

Stienstra, R., Netea-Maier, R.T., Riksen, N.P., Joosten, L.A.B., and Netea, M.G. (2017). Specific and Complex Reprogramming of Cellular Metabolism in Myeloid Cells during Innate Immune Responses. Cell Metab *26*, 142-156.

Tacke, F., Alvarez, D., Kaplan, T.J., Jakubzick, C., Spanbroek, R., Llodra, J., Garin, A., Liu, J., Mack, M., van Rooijen, N., et al. (2007). Monocyte subsets differentially employ CCR2, CCR5, and CX3CR1 to accumulate within atherosclerotic plaques. The Journal of clinical investigation *117*, 185-194.

Tan, Y.Y., Gast, G.C., and van der Schouw, Y.T. (2010). Gender differences in risk factors for coronary heart disease. Maturitas *65*, 149-160.

Taneja, V. (2018). Sex Hormones Determine Immune Response. Front Immunol *9*, 1931.

Tibshirani, R. (1996). Regression shrinkage and selection via the lasso. J. R. Statist. Soc. B *58*, 267–288.

van der Windt, G.J., Everts, B., Chang, C.H., Curtis, J.D., Freitas, T.C., Amiel, E., Pearce, E.J., and Pearce, E.L. (2012). Mitochondrial respiratory capacity is a critical regulator of CD8+ T cell memory development. Immunity *36*, 68-78.

Vats, D., Mukundan, L., Odegaard, J.I., Zhang, L., Smith, K.L., Morel, C.R., Wagner, R.A., Greaves, D.R., Murray, P.J., and Chawla, A. (2006). Oxidative metabolism and PGC-1beta attenuate macrophage-mediated inflammation. Cell Metab *4*, 13-24.

Vernia, S., Cavanagh-Kyros, J., Barrett, T., Jung, D.Y., Kim, J.K., and Davis, R.J. (2013). Diet-induced obesity mediated by the JNK/DIO2 signal transduction pathway. Genes Dev *27*, 2345-2355.

Willeit, J., Kiechl, S., Egger, G., Oberhollenzer, M., Oberhollenzer, F., Muggeo, M., Poewe, W., and Bonora, E. (1997). The role of insulin in age-related sex differences of cardiovascular risk profile and morbidity. Atherosclerosis *130*, 183-189.

Winn, N.C., Jurrissen, T.J., Grunewald, Z.I., Cunningham, R.P., Woodford, M.L., Kanaley, J.A., Lubahn, D.B., Manrique-Acevedo, C., Rector, R.S., Vieira-Potter, V.J., et al. (2019). Estrogen receptor-alpha signaling maintains immunometabolic function in males and is obligatory for exercise-induced amelioration of nonalcoholic fatty liver. Am J Physiol Endocrinol Metab *316*, E156-E167.

Wiria, A.E., Hamid, F., Wammes, L.J., Prasetyani, M.A., Dekkers, O.M., May, L., Kaisar, M.M., Verweij, J.J., Guigas, B., Partono, F., et al. (2015). Infection with Soil-Transmitted Helminths Is Associated with Increased Insulin Sensitivity. PloS one *10*, e0127746.

Wolde, M., Berhe, N., Medhin, G., Chala, F., van Die, I., and Tsegaye, A. (2019). Inverse Associations of Schistosoma mansoni Infection and Metabolic Syndromes in Humans: A Cross-Sectional Study in Northeast Ethiopia. Microbiol Insights *12*, 1178636119849934.

Wolfs, I.M., Stoger, J.L., Goossens, P., Pottgens, C., Gijbels, M.J., Wijnands, E., van der Vorst, E.P., van Gorp, P., Beckers, L., Engel, D., et al. (2014). Reprogramming macrophages to an anti-inflammatory phenotype by helminth antigens reduces murine atherosclerosis. FASEB J *28*, 288-299.

Wong, N.D., Zhao, Y., Patel, R., Patao, C., Malik, S., Bertoni, A.G., Correa, A., Folsom, A.R., Kachroo, S., Mukherjee, J., et al. (2016). Cardiovascular Risk Factor Targets and Cardiovascular Disease Event Risk in Diabetes: A Pooling Project of the Atherosclerosis Risk in Communities Study, Multi-Ethnic Study of Atherosclerosis, and Jackson Heart Study. Diabetes Care *39*, 668-676.

Zhou, Z., Subramanian, P., Sevilmis, G., Globke, B., Soehnlein, O., Karshovska, E., Megens, R., Heyll, K., Chun, J., Saulnier-Blache, J.S., et al. (2011). Lipoprotein-derived lysophosphatidic acid promotes atherosclerosis by releasing CXCL1 from the endothelium. Cell Metab *13*, 592-600.

Zou, H.a.H., T (2005). Regularization and variable selection via the elastic net. Journal of the Royal Statistical Society *67*, 301-320.

Figure legends

Figure 1. Bone marrow derived macrophages (BMDM) from ApoE$^{-/-}$ male *S. mansoni* infected mice exhibit increased oxygen consumption and mitochondria mass. ApoE$^{-/-}$ male

were fed HFD for 10 days before infection with *S. mansoni*. Ten weeks post infection mice were sacrificed and bone marrow cells were harvested and cultured for 7 days under M-CSF. (A) SeaHorse assay results for OCR of BMDC from infected and uninfected ApoE$^{-/-}$ males in basal conditions and in response to mitochondrial inhibitors. (B) Quantification (in picomoles per minute) of the basal oxygen consumption of BMDM from uninfected or infected ApoE$^{-/-}$ HFD male mice. (C) Quantification of the spare respiratory capacity of BMDM from uninfected or infected ApoE$^{-/-}$ HFD male mice (D) Extracellular acidification rate of BMDM from male uninfected or infected ApoE$^{-/-}$. (E) Oil Red O relative staining in BMDM from ApoE$^{-/-}$ mice (F) MitoTracker Red Deep Stain measure by flow cytometry in BMDM from ApoE$^{-/-}$ mice. SeaHorse assay analysis were performed the Seahorse XFe96 instrument. *$p < 0.05$; **$p < 0.01$; ***$p < 0.001$. Graphs are representative of multiple experiments (2-3), with n>4 per group.

Figure 2.

BMDM from male *S. mansoni* infected HFD ApoE$^{-/-}$ mice have increased TCA cycle usage and significantly reduced cholesterol esters. A-E) Mϕ were differentiated from bone marrow of 10-week infected animals with M-CSF in a 7-day culture in normal glucose and then switched to ^{13}C-labeled glucose for 24 hours. F-H) Mϕs were differentiated with M-CSF in a 7-day culture and then total cellular lipids were extracted and analyzed via LC-MS based lipidomic analysis. F) PLS-DA derived score from HFD Infected and HFD Uninfected BMDM. G) Plot of lipid species from the BMDM of infected and uninfected males on HFD, significantly altered lipid species are red and labeled. H)Table of statistical analysis of VIP I) Box whisker plot of normalized AUC of cholesterol ester species, which were identified as VIP compounds from the PLS-DA analysis. J-L) Bone marrow macrophages were differentiated with M-CSF and mRNA sequenced via RNASeq. J) Volcano plot of significantly differentially expressed genes between

BMDM from *S. mansoni* infected uninfected mice. K) iPathway analysis showed distinct profiles in BMDM from *S. mansoni* infected, mice. L,M) Total RNA was extracted from biologically independent BMDM differentiated in M-CSF for Real-time PCR validation of mgll and slc1a3 regulation.

Data in A-I are representative of 3 experiments with 4-6 mice per group in each experiment. Data in J and K are representative of sequencing of 2 biologically independent experiments with 5-6 mice per group. Data in L are from 2 biologically independent experiments with 4-6 mice per group.

Figure 3

***S. mansoni* infection does not protect females from metabolic disease despite inducing alternative activation in hepatic macrophages**. (A-B) Total body weight and glucose tolerance test (GTT) at 10 weeks post-infection. GTT values were analyzed by Area Under the Curve and graphed using GraphPad Prims. (C) (D) Flow cytometry analysis of alternative activation markers CD206 and CD302 in perfused and digested livers gated on hepatic macrophages ($CD45^+CD64^+MertK^+$) Arg-1 expression in hepatic macrophages from uninfected and infected $ApoE^{-/-}$ mice Nos-2 expression by flow cytometry in hepatic macrophages 10 weeks post infection. (E) Ly6C expression in monocyte from peripheral blood mononuclear cells (PBMC) at 10-week post infection by flow cytometry (F) MitoTracker Red in $CD115^+$ monocytes from PBMC at 10 weeks post immunization in uninfected and infected $ApoE^{-/-}$ mice. (G) Total cell counts from bone marrow cells utilizing trypan-blue discrimination of apoptotic cells (H) Percentages of CMP ($Lin^-CD127^-c\text{-}Kit^+Sca\text{-}1^-CD34^+CD16/32^{low}$) and GMP ($Lin^-CD127^-c\text{-}Kit^+Sca\text{-}1^-CD34^+CD16/32^{hi}$) (I) CMP cell counts in bone marrow $ApoE^{-/-}$ (J) GMP cell counts 10

week post infection in ApoE$^{-/-}$ mice (K) Flow cytometry analysis of MDP defined as Lin^{-}c-Kit^{+}Sca-1^{-}FcγR^{low}CD34^{+}CD115^{+} (L) MDP cell counts in ApoE$^{-/-}$uninfected and infected male mice. Graphs are representative from experiments that were performed 3-4 times with n>4. Exception is MitoTracker data, which was performed twice, with n>4. Statistical analysis was done using unpaired Student's t test, *$p < 0.05$; **$p < 0.01$.

Figure 4.

***S. mansoni* infection induces sex-specific modulation of oxygen consumption and beta-oxidation in BMDM.** (A-C) oxygen consumption rate and spare respiratory capacity were measured at steady state. D-F) BMDM palmitate dependent oxygen consumption and spare respiratory capacity was measured in glucose limiting conditions. G) Oil Red O relative staining in BMDM from ApoE$^{-/-}$ mice (H) MitoTracker Red Deep Stain measure by flow cytometry in BMDM from ApoE$^{-/-}$ mice. SeaHorse assay analysis were performed the Seahorse XFe96 instrument. *$p < 0.05$; **$p < 0.01$; ***$p < 0.001$. Graphs are representative of multiple experiments (2-3), with n>4 per group.

Figure 5.

***S. mansoni* infection induces significantly different cellular lipid profiles in BMDM from HFD female and male ApoE$^{-/-}$ mice.** A) PLS-DA derived score of LC-MS based lipidomic analysis of BMDM from HFD Infected females vs males. B) Box whisker plot of normalized AUC of cholesterol ester species, between female and male infected and uninfected HFD ApoE$^{-/-}$ mice. C) PLS-DA derived score from Female HFD Infected and uninfected BMDM. D) Dot plot of lipid species identified in BMDM from infected and uninfected female ApoE$^{-/-}$ mice on HFD,

1148 significant lipid species are represented by red dots and labeled. E) Relative quantitation of BMP
1149 compounds in BMDM from male and female animals with and without *S. man*soni infection. F-I)
1150 Macrophages were differentiated with M-CSF in a 7-day culture with normal glucose and serum,
1151 and then switched to ^{13}C-labeled palmitate in dialyzed serum for 36 hours. J-N) Culture
1152 supernatants from BMDM stimulated with LPS for 24 hours were assayed for
1153 chemokines/cytokines. Data in A-E and J-N are representative of 2 biologically independent
1154 experiments with 4-8 mice per group. F-I are one experiment with 5-6 mice per group.
1155
1156

1157

1158 Figure 6.

1159 ***S. mansoni* infection differentially regulates the transcriptomes of BMDM from female and**
1160 **male ApoE$^{-/-}$ mice**. (A) Venn diagram showing upregulated genes in males only, independently
1161 of infection state and pathway analysis corresponding to the identified genes. (B) Venn diagram
1162 and pathway analysis of differentially expressed genes in males compared to females. (C) Gene
1163 ontology map of differentially expressed genes in response to *S. mansoni* infection in male
1164 compared to female ApoE $^{-/-}$ mice on HFD. Sequencing data are from one experiment with 5-6
1165 mice per group.

1166

1167 **Figure 7. *S. mansoni* induced modulation of male macrophage metabolism is long-lived in**
1168 **the absence of antigen.** Bone marrow from 10-week *S. mansoni* infected or control ApoE-/-
1169 mice on HFD was transferred into busulfan treated ApoE$^{-/-}$ recipients on HFD. A,B) Glucose
1170 tolerance test (GTT) at 10 weeks post-infection. GTT values were analyzed by Area Under the
1171 Curve and graphed using GraphPad Prism. C-E) Oxygen consumption rate and spare respiratory

1172 capacity were measured at steady state in 7day BMDM. F) MitoTracker Red Deep Stain measure

1173 by flow cytometry in BMDM. Data is two combined experiments 7-8 animals per group.

1174 Statistical analysis was done using Welch's t-tests.

1175

Figure 1

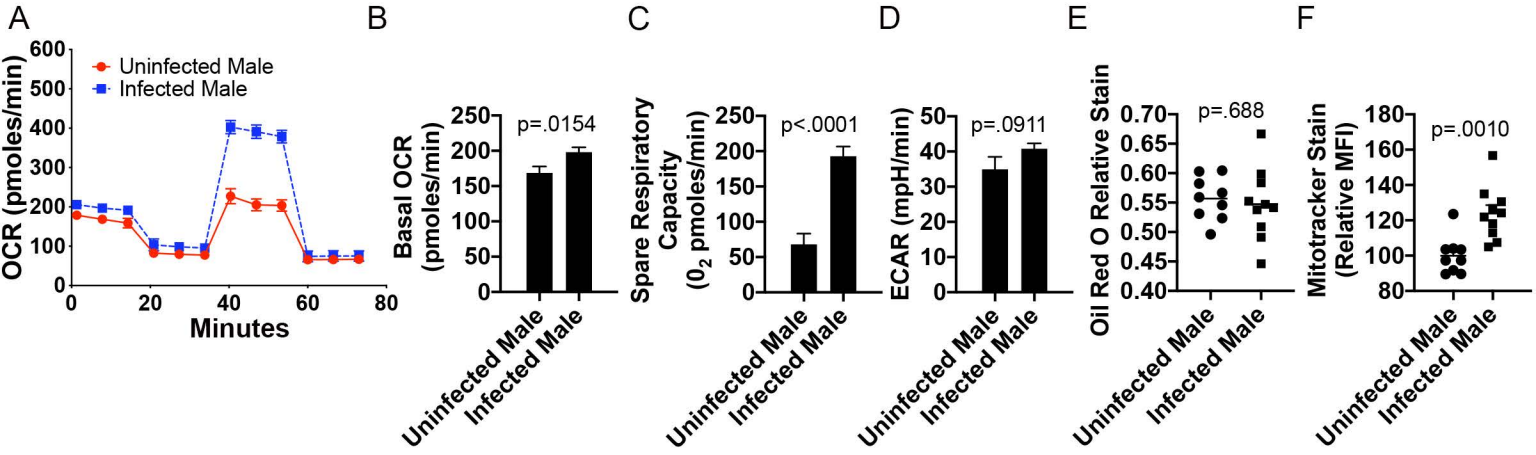
A
B
C
D
E
F
Uninfected Male
Infected Male
OCR (pmoles/min)
Minutes
Basal OCR (pmoles/min)
p=.0154
Spare Respiratory Capacity (0_2 pmoles/min)
p<.0001
ECAR (mpH/min)
p=.0911
Oil Red O Relative Stain
p=.688
Mitotracker Stain (Relative MFI)
p=.0010

Figure 2

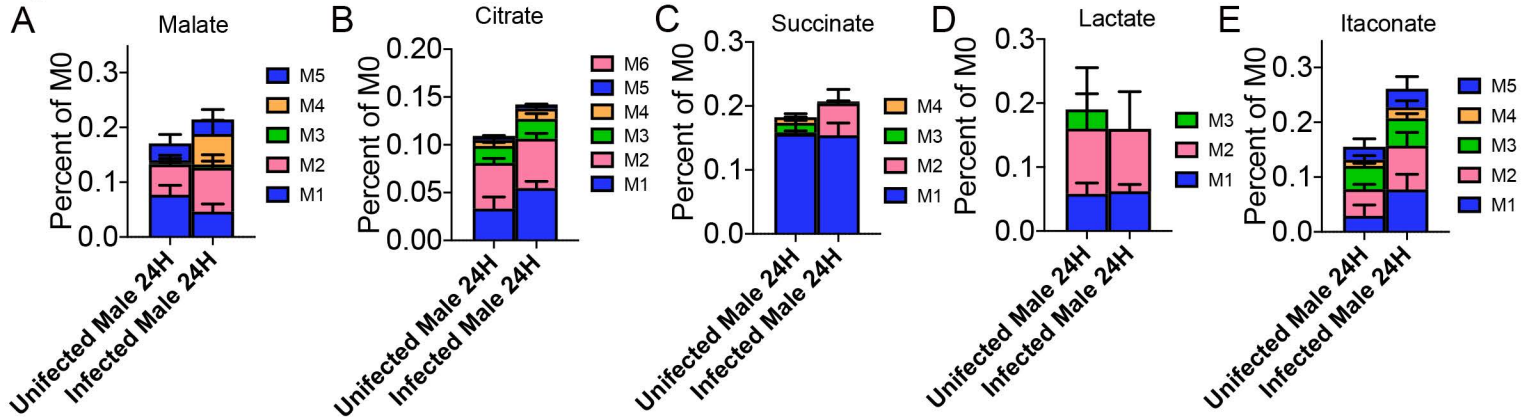

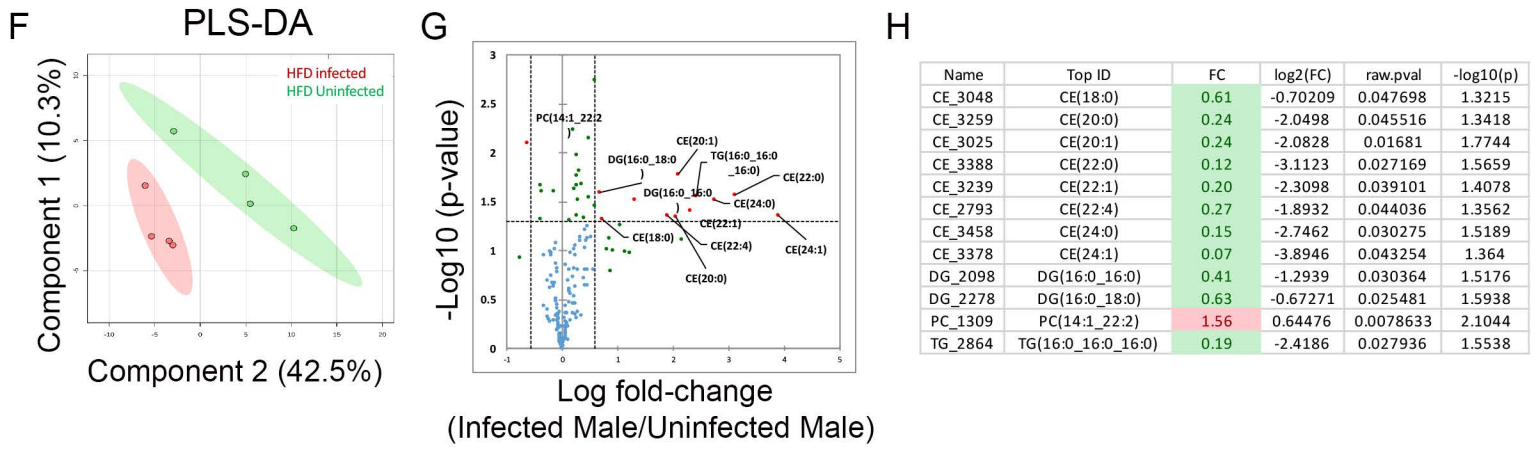

H

Name	Top ID	FC	log2(FC)	raw.pval	-log10(p)
CE_3048	CE(18:0)	0.61	-0.70209	0.047698	1.3215
CE_3259	CE(20:0)	0.24	-2.0498	0.045516	1.3418
CE_3025	CE(20:1)	0.24	-2.0828	0.01681	1.7744
CE_3388	CE(22:0)	0.12	-3.1123	0.027169	1.5659
CE_3239	CE(22:1)	0.20	-2.3098	0.039101	1.4078
CE_2793	CE(22:4)	0.27	-1.8932	0.044036	1.3562
CE_3458	CE(24:0)	0.15	-2.7462	0.030275	1.5189
CE_3378	CE(24:1)	0.07	-3.8946	0.043254	1.364
DG_2098	DG(16:0_16:0)	0.41	-1.2939	0.030364	1.5176
DG_2278	DG(16:0_18:0)	0.63	-0.67271	0.025481	1.5938
PC_1309	PC(14:1_22:2)	1.56	0.64476	0.0078633	2.1044
TG_2864	TG(16:0_16:0_16:0)	0.19	-2.4186	0.027936	1.5538

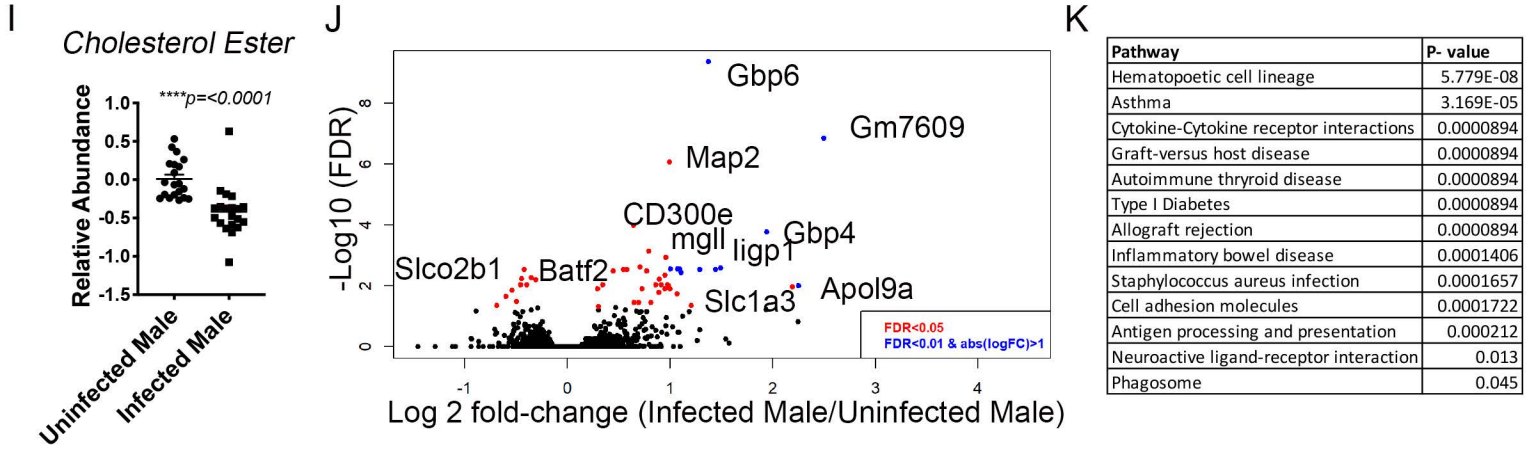

K

Pathway	P- value
Hematopoetic cell lineage	5.779E-08
Asthma	3.169E-05
Cytokine-Cytokine receptor interactions	0.0000894
Graft-versus host disease	0.0000894
Autoimmune thryroid disease	0.0000894
Type I Diabetes	0.0000894
Allograft rejection	0.0000894
Inflammatory bowel disease	0.0001406
Staphylococcus aureus infection	0.0001657
Cell adhesion molecules	0.0001722
Antigen processing and presentation	0.000212
Neuroactive ligand-receptor interaction	0.013
Phagosome	0.045

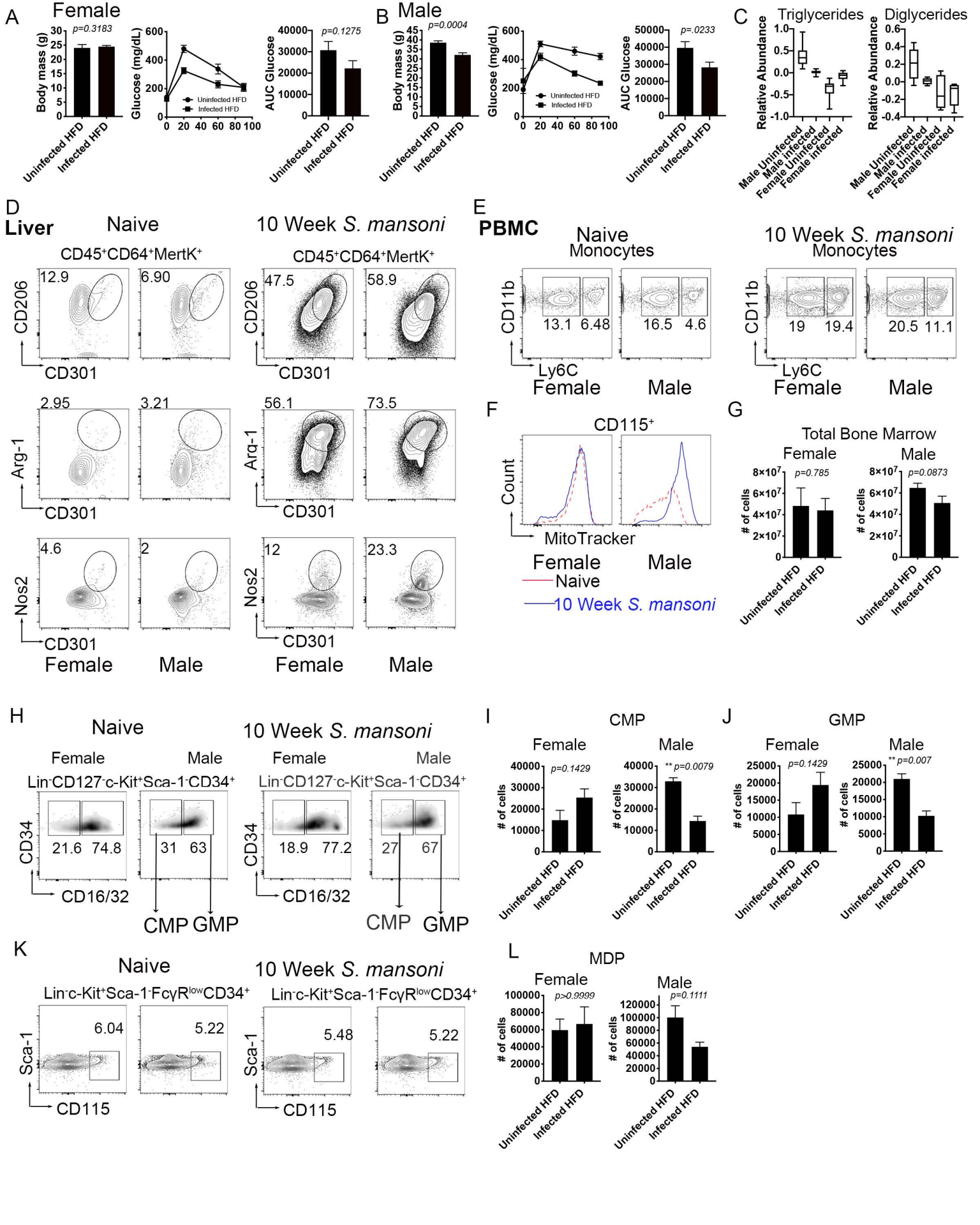
A
Female
Body mass (g)
p=0.3183
Uninfected HFD
Infected HFD
Glucose (mg/dL)
AUC Glucose
p=0.1275
B
Male
p=0.0004
p=.0233
C
Triglycerides
Diglycerides
Relative Abundance
Male Uninfected
Male Infected
Female Uninfected
Female Infected
D
Liver
Naive
10 Week S. mansoni
CD45+CD64+MertK+
CD206
CD301
12.9
6.90
47.5
58.9
Arg-1
2.95
3.21
56.1
73.5
Nos2
4.6
2
12
23.3
Female
Male
E
PBMC
Monocytes
CD11b
Ly6C
13.1
6.48
16.5
4.6
19
19.4
20.5
11.1
F
CD115+
Count
MitoTracker
Naive
10 Week S. mansoni
G
Total Bone Marrow
# of cells
p=0.785
p=0.0873
H
Lin-CD127-c-Kit+Sca-1-CD34+
CD34
CD16/32
21.6
74.8
31
63
18.9
77.2
27
67
CMP
GMP
I
CMP
p=0.1429
** p=0.0079
J
GMP
p=0.1429
** p=0.007
K
Lin-c-Kit+Sca-1-FcγRlowCD34+
Sca-1
CD115
6.04
5.22
5.48
5.22
L
MDP
p>0.9999
p=0.1111

Figure 4

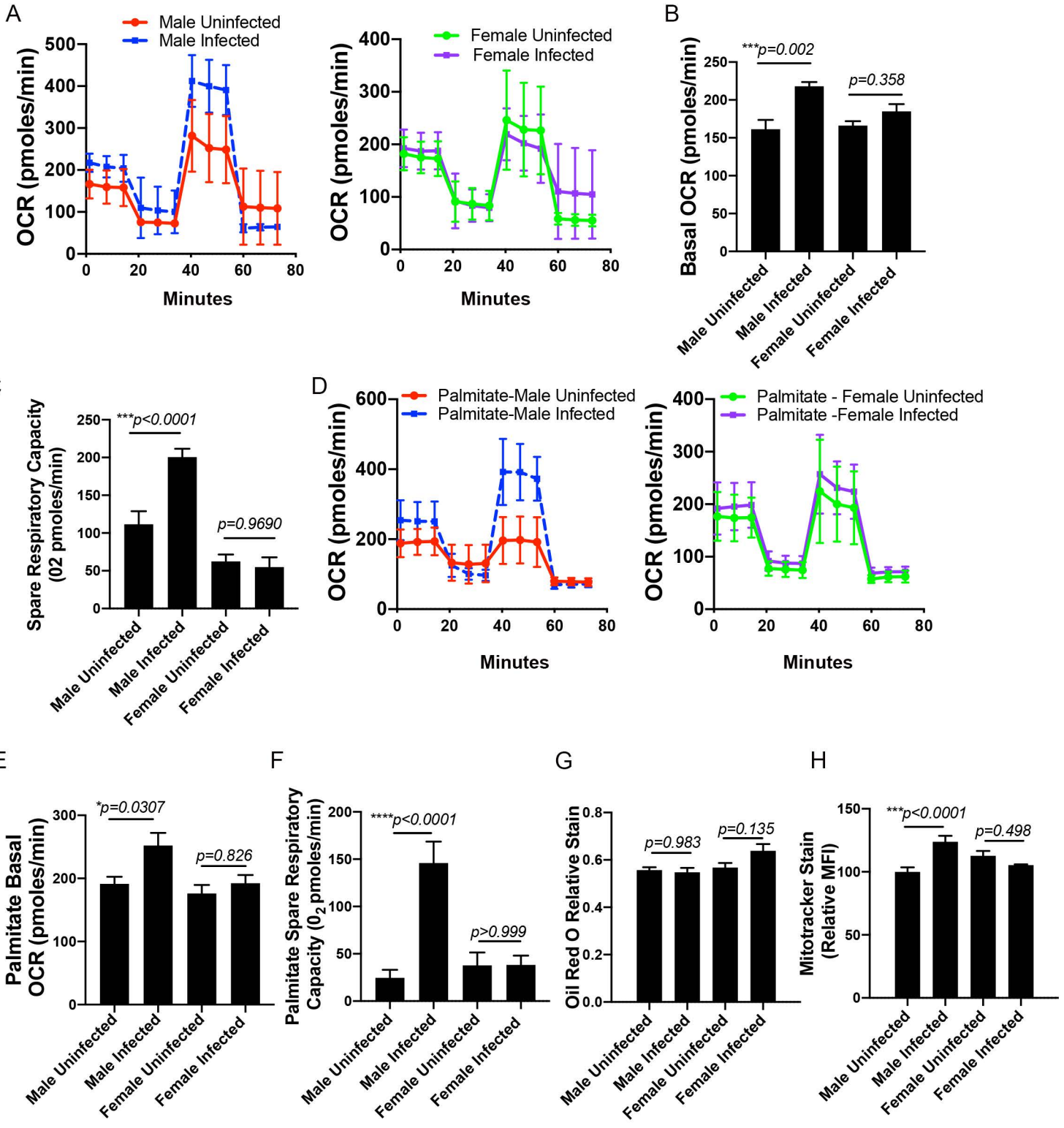
A
Male Uninfected
Male Infected
OCR (pmoles/min)
Minutes
Female Uninfected
Female Infected
B
***p=0.002
p=0.358
Basal OCR (pmoles/min)
Male Uninfected
Male Infected
Female Uninfected
Female Infected
C
***p<0.0001
p=0.9690
Spare Respiratory Capacity (02 pmoles/min)
D
Palmitate-Male Uninfected
Palmitate-Male Infected
Palmitate - Female Uninfected
Palmitate -Female Infected
E
*p=0.0307
p=0.826
Palmitate Basal OCR (pmoles/min)
F
****p<0.0001
p>0.999
Palmitate Spare Respiratory Capacity (02 pmoles/min)
G
p=0.983
p=0.135
Oil Red O Relative Stain
H
***p<0.0001
p=0.498
Mitotracker Stain (Relative MFI)

Figure 5

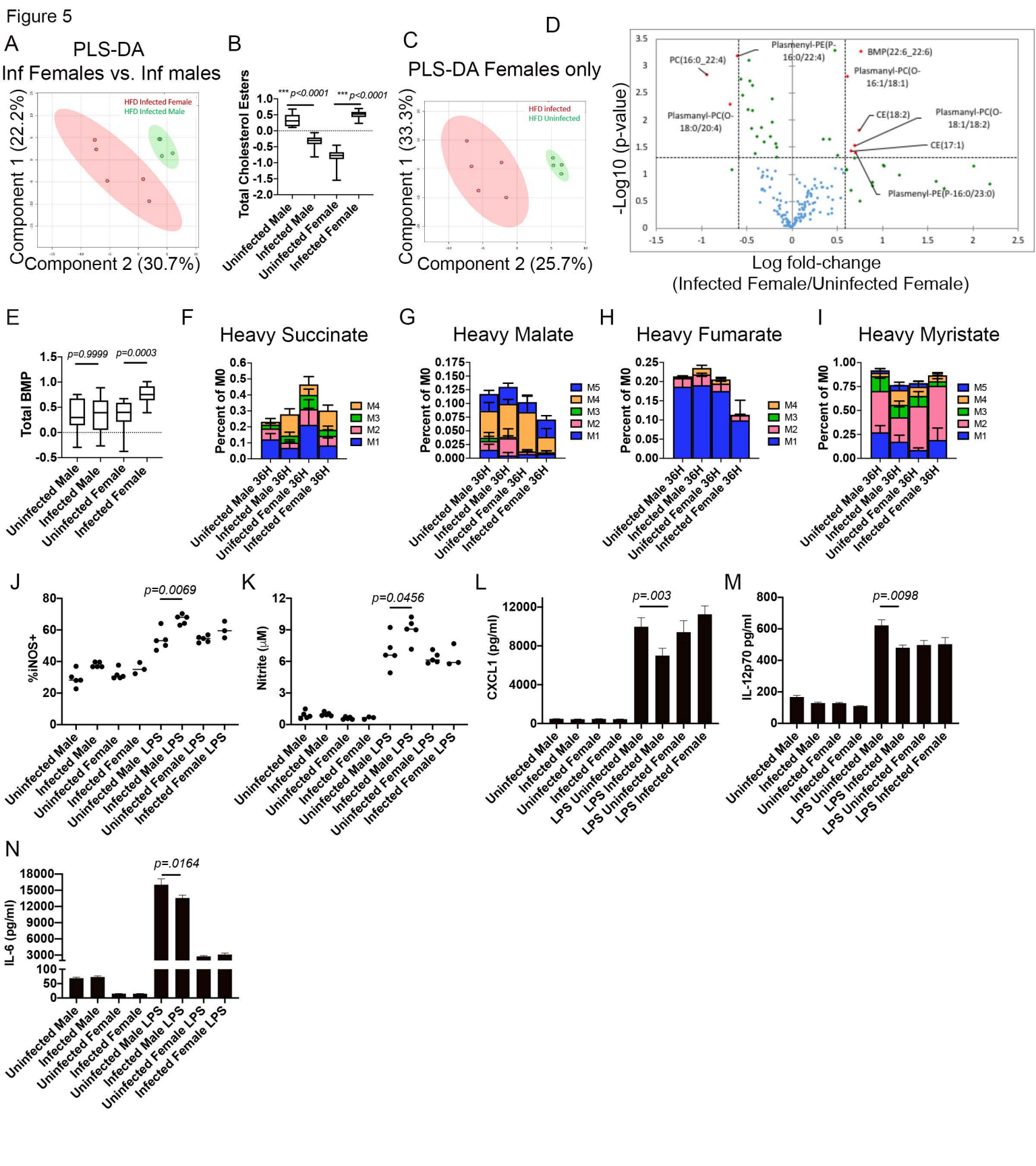
A
PLS-DA
Inf Females vs. Inf males
HFD Infected Female
HFD Infected Male
Component 1 (22.2%)
Component 2 (30.7%)
B
Total Cholesterol Esters
***p<0.0001
***p<0.0001
Uninfected Male
Infected Male
Uninfected Female
Infected Female
C
PLS-DA Females only
HFD infected
HFD Uninfected
Component 1 (33.3%)
Component 2 (25.7%)
D
-Log10 (p-value)
Log fold-change
(Infected Female/Uninfected Female)
Plasmenyl-PE(P-16:0/22:4)
BMP(22:6_22:6)
PC(16:0_22:4)
Plasmanyl-PC(O-16:1/18:1)
Plasmanyl-PC(O-18:0/20:4)
CE(18:2)
Plasmanyl-PC(O-18:1/18:2)
CE(17:1)
Plasmenyl-PE(P-16:0/23:0)
E
Total BMP
p=0.9999
p=0.0003
F
Heavy Succinate
Percent of M0
G
Heavy Malate
H
Heavy Fumarate
I
Heavy Myristate
M5
M4
M3
M2
M1
Uninfected Male 36H
Infected Male 36H
Uninfected Female 36H
Infected Female 36H
J
%iNOS+
p=0.0069
K
Nitrite (μM)
p=0.0456
L
CXCL1 (pg/ml)
p=.003
M
IL-12p70 pg/ml
p=.0098
Uninfected Male
Infected Male
Uninfected Female
Infected Female
Uninfected Male LPS
Infected Male LPS
Uninfected Female LPS
Infected Female LPS
N
IL-6 (pg/ml)
p=.0164

Figure 6

A Upregulated genes in males

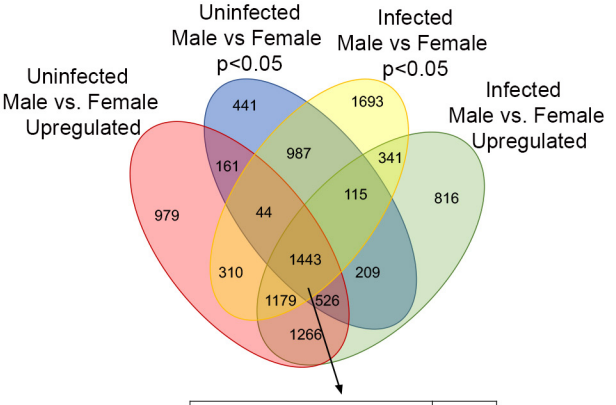

Pathways	Number of genes
Metabolism	238
Innate Immune System	216
Gene expression	183
Metabolism of proteins	149
Class I MHC Mediated Antigen Processing	85
Cell cycle	76
Vesicle mediated transport	72
Unassigned	63
Regulation of TP53 activity	52
NK-KappaB Signaling	47
DNA Double-strand break repair	42
Organelle biogenesis and maintenance	42
TNFR1 Pathway	31

B Differential regulation in male vs. female

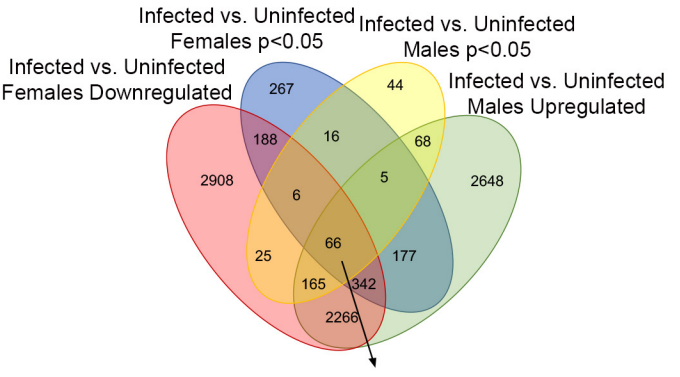

Pathways	Number of genes
Unassigned	31
Metabolism	10
Hemostasis	6
Adaptive immune system	2
Collagen degradation	2
Developmental biology	2
Metabolism of proteins	2
Neurotransmitter receptors and postsynaptic signal transmission	2
ROS and RNS production in phagocytes	2
Signal transduction	2

C Gene Ontology Map

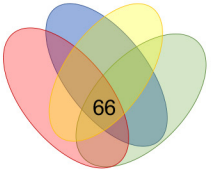

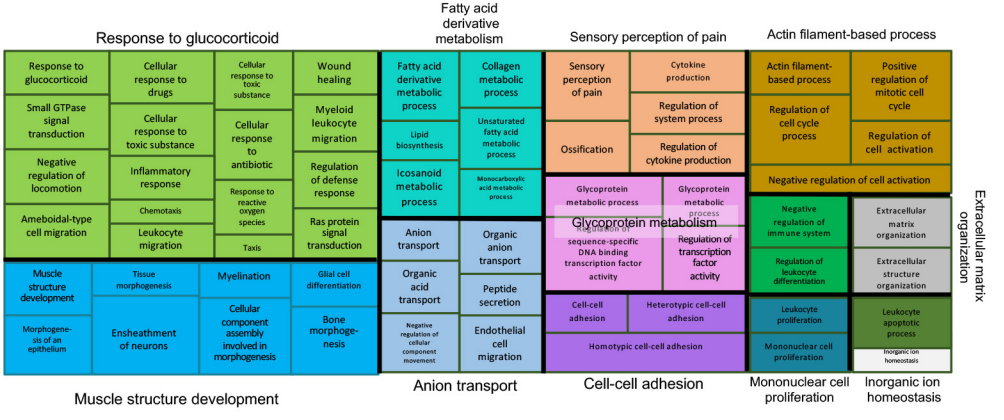

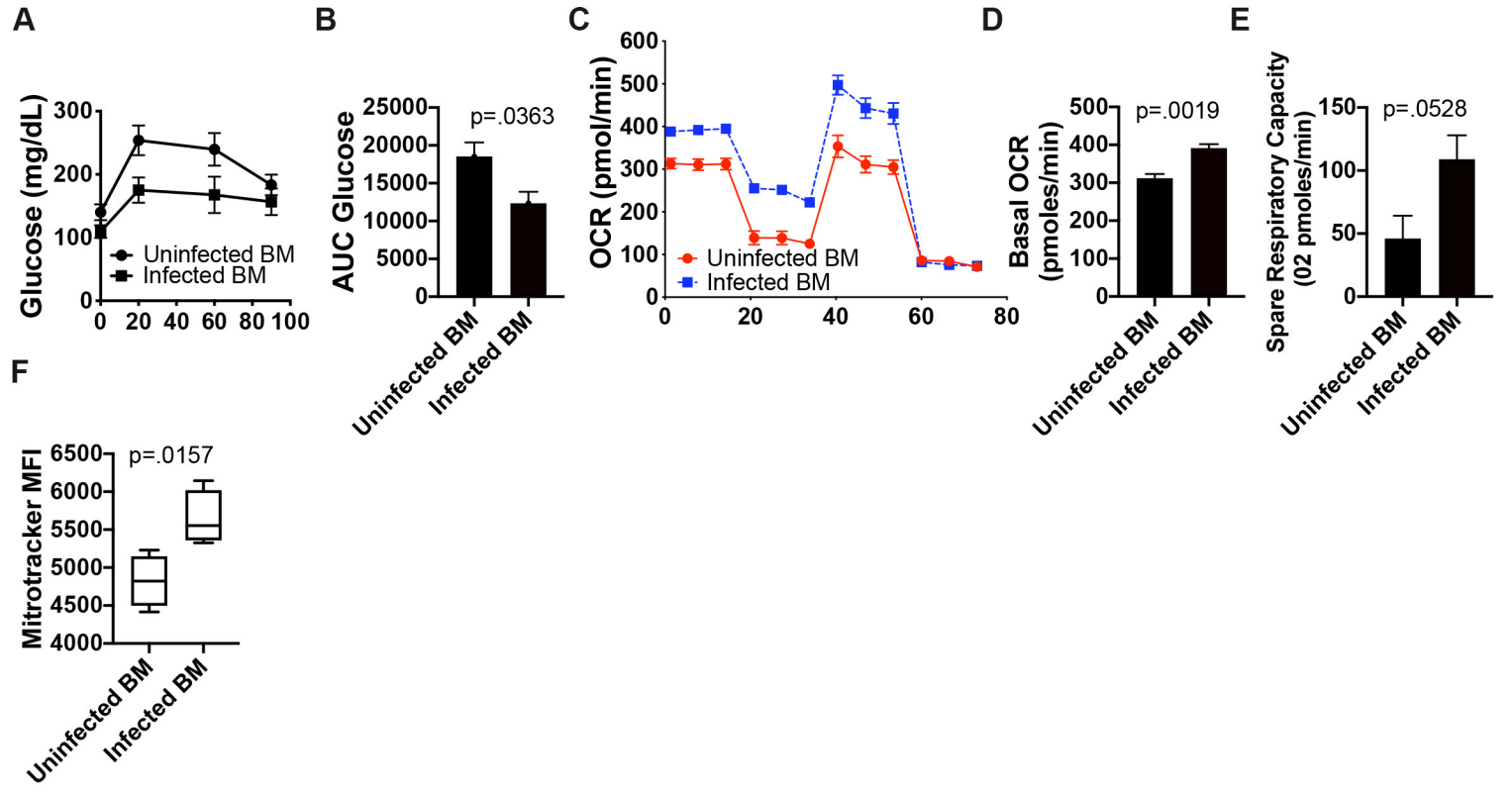
A
Glucose (mg/dL)
300
200
100
0
0 20 40 60 80 100
Uninfected BM
Infected BM
B
AUC Glucose
25000
20000
15000
10000
5000
0
p=.0363
Uninfected BM
Infected BM
C
OCR (pmol/min)
600
500
400
300
200
100
0
0 20 40 60 80
Uninfected BM
Infected BM
D
Basal OCR (pmoles/min)
500
400
300
200
100
0
p=.0019
Uninfected BM
Infected BM
E
Spare Respiratory Capacity (02 pmoles/min)
150
100
50
0
p=.0528
Uninfected BM
Infected BM
F
Mitrotracker MFI
6500
6000
5500
5000
4500
4000
p=.0157
Uninfected BM
Infected BM